DEVELOPMENT OF GOLD NANOPARTICLE CONJUGATED POLYETHYLENE TEREPHTHALATE FOR IMPROVED BIOCOMPATIBLITY IN HERNIA REPAIR MATERIALS

A Thesis presented to

the Faculty of the Graduate School

at the University of Missouri

In Partial Fulfillment

of the Requirements for the Degree

Master of Science

---

by

ONA WHELOVE

Dr. Sheila Grant, Thesis Supervisor

DECEMBER 2010

The undersigned, appointed by the dean of the Graduate School, have examined the thesis entitled

DEVELOPMENT OF GOLD NANOPARTICLE CONJUGATED POLYETHYLENE TEREPHTHALATE FOR IMPROVED BIOCOMPATIBLITY IN HERNIA REPAIR MATERIALS

presented by Ona Whelove,

a candidate for the degree of Master of Science,

and hereby certify that, in their opinion, it is worthy of acceptance.

_____

Dr. Sheila Grant, Biological Engineering Department

_____

Dr. John Viator, Biological Engineering Department

_____

Dr. Sharon Bachman, Department of Surgery

_____

Dr. Derek Fox, Department of Veterinary Medicine and Surgery

ACKNOWLEDGEMENTS

I would like to thank Dr. Sheila Grant for allowing me the opportunity to work in her research laboratory both in undergraduate and graduate school. It was through hands-on experience in her biomaterials lab that I developed a passion for biomedical engineering and a desire to pursue a career in the research and development field. Dr. Grant's constant inspiration and plethora of expertise has aided me in my graduate research and allowed me to seek opportunities that otherwise would not be possible.

In addition to Dr. Grant, I would like to acknowledge my committee members, Dr. Sharon Bachman, Dr. Derek Fox, and Dr. John Viator, for dedicating time out of their extremely busy schedules to guide and give feedback on my research project.

I would also like to thank Matthew Cozad for taking time to mentor me on how to perform laboratory procedures and properly use laboratory equipment. His knowledge and extremely detailed protocols have assisted me with my research and prevented much frustration throughout my graduate studies.

Additionally, I would like to thank Dave Grant for assisting in my pursuit of a career in industry, as well as all the members of the Grant lab for promoting a positive and friendly environment, which has undoubtedly made my time as a graduate student much more enjoyable.

TABLE OF CONTENTS

Appendix

LIST OF FIGURES

Figure Page

LIST OF TABLES

Table Page

DEVELOPMENT OF GOLD NANOPARTICLE CONJUGATED POLYETHYLENE TEREPHTHALATE FOR IMPROVED BIOCOMPATIBLITY IN HERNIA REPAIR MATERIALS

Ona Whelove

Dr. Sheila Grant, Thesis Supervisor

ABSTRACT

Synthetic biomaterials are currently a popular choice for use in many surgical soft tissue repair applications. Polyethylene terephthalate (PET) is an example of such material that has been used, more specifically, for hernia repair. PET mesh is one of the top choices for hernia repair due to its flexibility, porosity, mechanical strength, and relative inertness; however, explanted PET hernia meshes have shown signs of degradation, which can cause complications with tissue compatibility and increase the chance for recurrence when used as a biomaterial implant for extended periods of time. In this study, the effects of modifying the PET surface, through chemical functionalization and gold nanoparticle (AuNP) conjugation, were investigated. Fourier transform infrared spectroscopy (FT-IR), scanning electron microscopy (SEM), energy dispersive spectroscopy (EDS), and differential scanning calorimetry (DSC) were used to characterize the modified PET in comparison to pristine PET. Results from these studies showed that the PET mesh surface could be successfully functionalized and cross-linked with AuNP while maintaining the physical and thermal properties of pristine PET. Cell culture assays, including WST-1 cell proliferation assays, reactive oxygen species (ROS) assays, and antimicrobial studies, were performed to investigate *in vitro* performances of the modified PET mesh.

CHAPTER 1
LITERATURE REVIEW

1.1 Introduction to Hernia Repair

1.1.1 Hernia background

A hernia occurs when the connective tissue over the abdominal muscles, called the fascia, breaks down. This can result in part of an internal organ or tissue being about to protrude through the weakness or tear in the surrounding muscular wall. There are two major types of hernia: ventral hernias and inguinal hernias. Ventral hernias can develop in various locations in the abdomen, including the navel, while inguinal hernias occur in the groin. Hernias can also occur at sites of previous surgical incision. Hernia repair is currently one of the most commonly performed surgical procedures; resulting in a plethora of different techniques and repair materials for surgeons to select from. (Bringman et al., 2010)

Originally, surgical hernia repair was performed by re-approximating the tissue and suturing the weakness in the muscular wall to keep the protrusion contained. This primary repair method can still be used to repair some types of hernias; however, the sutured area remains in tension, causing patients with large, abdominal hernias to experience a high rate of recurrence. (Voskerician et al., 2010; Grant and Ramshaw, 2010) Because of this, tension-free repair using a synthetic mesh patch has become the standard in abdominal hernia surgeries. The first hernia mesh was introduced by Usher *et al.* in 1958 and since then, mesh use has increased to over one million per year

worldwide. (Brown and Finch, 2010) While use of a synthetic mesh decreases the probability for hernia recurrence, it increases the amount of foreign material that must be implanted into the body and therefore increases the chance for complications due to foreign body response.

1.1.2 Hernia materials

An ideal hernia mesh should be biologically inert and exhibit good flexibility, elasticity, and mechanical strength. It should retain these properties *in vivo,* avoiding mesh degradation, contraction, and stiffening. The mesh should also promote tissue in-growth, while reducing inflammatory response, infection risk, and tissue adhesions. Because hernias occur in people of all ages, sizes, and medical backgrounds, a surgeon needs to be able to select a mesh with specific characteristics based on the individual needs of the patient. Some factors that have been shown to affect the performance of hernia meshes are pore size, tensile strength, weight, biological reactivity, elasticity, constitution, and surface structure. (Bringman et al., 2010; Brown and Finch, 2010) In addition to these performance factors, the patient's genetics play a large role in his or her body's response to the implanted mesh. (Klinge et al., 1999)

The first hernia mesh, introduced by Francis Usher in 1958, was a basic polypropylene mesh. (Brown and Finch, 2010) Since then, several other materials have been used, including polyethylene terephthalate (PET), polytetrafluoroethylene (PTFE), polyglactin, and polyglycolic acid, as well as various biologic materials. In the ongoing effort to create the ideal hernia mesh, companies have produced numerous meshes

comprised of a various synthetic components. Table 1 gives a summary of some basic, synthetic hernia meshes currently on the market.

Table 1. Commercially available, individual material meshes for hernia repair.

Product	Company	Material	Description
ProLite™	Atrium	polypropylene	Monofilament mesh with 2D flexibility, available in heavyweight and lightweight
3D Max™	Bard	polypropylene	3D, large pore, knitted mesh, available in heavyweight and lightweight
Dulex™	Bard	ePTFE	Microporous on one side and macroporous on the reverse side
Safil®	B. Braun	polyglycolic acid	Knitted, absorbable mesh
Premilene®	B. Braun	polypropylene	Monofilament mesh with large pores
Optilene®	B. Braun	polypropylene	Lightweight, large pore mesh with multidirectional elasticity
Omyra®	B. Braun	cPTFE	Condensed PTFE with a lightweight, macroporous structure
Parietex™ Flat sheet	Covidien	PET	Lightweight, macroporous mesh, available in 2D and 3D weaves
Parietex™ Lightweight	Covidien	PET	Monofilament, macroporous
Surgipro™	Covidien	polypropylene	Nonabsorbable, available in multifilament, monofilament, or open weave
Prolene™	Ethicon	polypropylene	Knitted, nonabsorbable filaments
Vicryl™	Ethicon	polyglactin	Absorbable mesh
Mersilene™	Ethicon	PET	Nonabsorbable, knitted mesh with large pores
Infinit®	Gore	PTFE	Monofilament, large pore, knitted mesh
Gore-Tex®	Gore	ePTFE	Smooth prosthetic patch with microporous structure

In addition to using a variety of individual materials for hernia meshes, companies have also produced several composite meshes, such as dual sided and coated materials. These hybrid meshes attempt to optimize more of the ideal characteristics of the "perfect" hernia mesh by selecting different materials based on the tissue that will be surrounding

the implant. Examples of some composite hernia meshes currently available are listed in Table 2.

Table 2. Commercially available composite hernia meshes.

Product	Company	Material	Description
Composix™	Bard	polypropylene/ePTFE	Lightweight polypropylene with overlap of ePTFE at the edges
Sepramesh™	Bard/Genzyme	polypropylene/sodium	Partially absorbable, large pore mesh with Seprafilm hydrogel coating
TiMesh®	Biomet	polypropylene/titanium	Monofilament, composite mesh, available in extra light, light, and strong
Parietex™ Composite	Covidien	PET/collagen	3D, knitted mesh with a collagen barrier on one side
Proceed™	Ethicon	polypropylene/cellulose	Large pore, monofilament mesh with a bioabsorbable component
Ultrapro™	Ethicon	Polypropylene / polyglecaprone	Lightweight, partially absorbable mesh
Dualmesh®	Gore	ePTFE	Two surface design with closed structure on one side and macroporous structure on the reverse, Dualmesh® Plus available with antimicrobial preservative agents
Mycromesh®	Gore	ePTFE	Microporous node and fibril structure with spaced macropores, Mycromesh® Plus available with antimicrobial preservative agents

When researching available hernia meshes, three polymers seem to dominate the industry: polypropylene, PET, and PTFE. Like most medical implants, when *in vivo*, each material exhibits some positive characteristics but at the expense of a different performance factor.

Polypropylene: Polypropylene is a thermoplastic polymer consisting of a main carbon chain with methyl side groups attached to the backbone. It has been used as a biomaterial for hernia repair due to its flexibility, strength, and chemical resistance; however, polypropylene is also hydrophobic and susceptible to oxidation, which has been shown to cause complications *in vivo*. In mesh fabrication, semi-crystalline polypropylene fibers are woven together to form monofilament or multifilament scaffolds. Traditional polypropylene hernia meshes are classified as heavyweight, dense, and microporous. They exhibit high mechanical strength and reduce the recurrence rate in comparison to primary suture repair. (Costello et al., 2007a) Heavyweight polypropylene meshes also cause large foreign body responses and thick fibrotic formation, resulting in restriction of movement and patient pain. (Brown and Finch, 2010) The increased immune response induced by polypropylene mesh implantation has been shown to increase secretion of byproducts, such as hydrogen peroxide, resulting in higher rates of oxidation and degradation of the mesh *in vivo*. (Costello et al., 2007b) Because of the consistent complications experienced with heavyweight polypropylene meshes, lightweight meshes with large pores were introduced. These macroporous meshes have been shown in literature to promote better tissue integration while reducing the foreign body reaction. (Eriksen et al., 2007) This results in less scar tissue formation, which allows the mesh to remain flexible *in vivo*, along with less secretion of oxidizing agents thus lowering the potential rate of mesh degradation.

Polytetrafluoroethylene: PTFE is a thermoplastic polymer comprised of carbon and fluorine molecules, and is classified as a heavyweight, dense material with a highly

crystalline structure. It has been used as a biomaterial in various medical devices because of its high strength, chemical inertness, and thermal stability. The chemical resistivity of PTFE allows it to perform well *in vivo* with respect to reduced material degradation and low risk for adhesions; however, its smooth surface does not promote tissue integration. (Brown and Finch, 2010) The poor integration prevents the biomaterial from being incorporated into the body and can result in scar tissue formation and mesh shrinkage, increasing the risk for hernia recurrence. When used for hernia repair, PTFE is typically stretched to create a microporous structure and is referred to as expanded PTFE (ePTFE). (Grant and Ramshaw, 2010) Recently, a monofilament, macroporous PTFE mesh has been developed to combine PTFE's desirable chemical inertness with enhanced tissue in-growth, lower infection risk, and reduced fibrosis.

Polyethylene terephthalate: PET is a thermoplastic polymer commonly referred to as polyester. Its semi-crystalline structure is of light-to-medium weight and density, making it slightly heavier than polypropylene but still much lighter than PTFE. PET has many applications, including various uses within the medical field such as cardiovascular repair, orthopaedic ligament reconstruction, and hernia repair. When fabricated as a hernia mesh, its synthetic fibers are woven into a macroporous pattern that can be either two or three-dimensional, as well as monofilament or multifilament. PET became increasingly popular as an option for hernia repair due to its superior performance as an anterior cruciate ligament (ACL) replacement, (Zieren et al., 2004) and has remained as one of the top three hernia mesh materials because of its high mechanical strength, flexibility, and relative inertness. (Li et al., 2007) It is also more hydrophilic than

polypropylene and PTFE, which allows it to promote better tissue in-growth when *in vivo*. (Voskerician et al., 2010) The main downfall of PET use in hernia repair has been its susceptibility to hydrolytic and oxidative degradation, causing its physical and chemical properties to be altered. (Voskerician et al., 2010; Grant and Ramshaw, 2010)

1.2 Biomaterial Surface Modifications

The synthetic biomaterials discussed in the previous section are commonly used in hernia repair due to their bulk material properties. Most complications that arise when these meshes are implanted are due to the cellular response of the surrounding tissue to the surface of the foreign mesh. Therefore, much research has been conducted focusing on surface modifications of synthetic hernia mesh materials to improve biocompatibility. Objectives of this area of research include promoting cell proliferation by increased surface hydrophilicity, surface functionalization, and conjugation of enzymes or proteins; as well as limiting foreign body response, infection, and adhesion formation through use of surface coatings and ion implantation. With its increasing popularity as a hernia mesh material and responsiveness to surface modifications, PET will be the material focused on in the following sections of this review.

1.2.1 Surface modifications to control cellular response

In literature, surface modification of synthetic hernia mesh material has been utilized to increase cell proliferation by a variety of methods. PET mesh, in particular,

has been modified by use of chemicals, plasma treatment, graft polymerization, and ultraviolet (UV) radiation, among others. (Zhang et al., 2008) For the purpose of controlling cellular response, the objective of PET surface modification is usually to achieve one of two goals: to increase surface hydrophilicity or to functionalize the surface for future conjugation to a different substance.

Surface modification of polymers by plasma treatment has been a popular research area for over 25 years. Clark and Wilson (1983) used hydrogen and oxygen plasma to functionalize the surface of PET, and a wide variety of plasma treatments are still being used in the biomedical field today. CO_2 plasma, among others, is commonly used to introduce carboxylic acid groups onto the surface of PET, resulting in increased surface hydrophilicity and thus, increased surface free energy. (Yang, L. et al., 2009) Many groups have shown good results with plasma modified PET for increased hydrophilicity and adhesion properties; however, plasma treatments also cause material degradation and have to be used in moderation to avoid hindering the bulk properties of PET. (Takke et al., 2009) Other methods have utilized plasma treatment in combination with UV radiation to graft functional groups to the surface, introducing conjugation sites for specific molecules. (Jingrun et al., 2008; Zhu et al., 2008) These techniques, commonly used on implantable biomaterials, combine physical modification with chemical cross-linking to more specifically control the characteristics of the PET surface.

Chemical modification of PET is another widely researched area for biomedical applications and can be used to gain more precise control of surface properties than physical modification methods. (Zhang et al., 2008) PET has been modified by numerous

combinations of chemicals, usually including strong acids or alkalis, which have the ability to break the ester bonds and introduce functional groups to the polymer surface. (Irena et al., 2009) In biomedical material research, cell response to various types of chemical modification has been investigated both *in vitro* and *in vivo*. Objectives of these modifications have been to improve cellular response by either increasing surface hydrophilicity or by conjugating the functionalized PET surface with biocompatibility-enhancing substances, such as biomolecules or nanomaterials.

Chemical modification processes, such as hydrolysis and aminolysis, are commonly used for PET surface modification and have been shown to increase the hydrophilicity of the polymer, as well as providing functional groups for binding in subsequent reactions. (Irena et al., 2009; Muthuvijayan et al., 2009) These processes have been proven to be efficient in increasing hydrophilicity and functionalizing the surface, (Liu et al., 2005) resulting in increased cell proliferation and attachment, (Zhang et al., 2008; Irena et al., 2009) without producing cytotoxic effects. However, hydrolysis and aminolysis have also been shown to cause bulk polymer deterioration, resulting in loss of mechanical strength and long-term durability of the biomaterial.

Carboxylation is another technique that has been performed to introduce functional groups to the surface of PET. (Yang, Z., et al., 2000) Recently, the mechanical properties of carboxylated PET were investigated and compared to those of hydrolyzed and aminolyzed PET. Carboxylated PET was shown to retain mechanical strength similar to that of unmodified PET, while the hydrolyzed and aminolyzed PET samples

showed significant losses of mechanical strength after their respective modifications. (Muthuvijayan et al., 2009)

1.2.2 Conjugations and coatings

In addition to the attempts of promoting tissue response to PET by enhancing its surface characteristics, conjugations of biomolecules and nanomaterials to the PET surface have been performed to further increase its biocompatibility. The substances to be conjugated are selected based on the area of the body in which the mesh will be implanted. Owing to the large market for PET as a cardiovascular repair material, much of the current research has been focused to improving proliferation of cells present in blood vessels; however, the techniques used could be further researched and potentially adapted for use in modifying PET for hernia repair. Liu et al. (2005) performed a multistep modification process by first hydrolyzing the PET surface and then using the carboxyl groups to adsorb chitosan and chondroitin sulfate in a layer-by-layer assembly to increase cytocompatibility for endothelial cells. L-arginine, an amino acid important for wound healing and immune response, has been cross-linked to PET and was shown to improve blood compatibility. (Liu et al., 2008; Liu et al., 2010) Jingrun et al. (2008) cross-linked albumin and gelatin to the PET surface and observed improved endothelial cell attachment and proliferation. (Jingrun et al., 2008)

With risk for infection at the biomaterial-tissue interface being a legitimate concern in hernia repair, research has also focused on surface modifications of implantable materials to decrease bacteria adhesion. Biomolecules with known

antimicrobial properties, as well as silver ions and nanomaterials, have been conjugated to PET surfaces and tested against bacteria commonly encountered at surgical wound sites. Li et al. (2007) modified PET using silver ion implantation and found a significant decrease in colony forming units (CFU) of *Staphylococcus epidermidis*, bacteria that commonly causes biofilms to form on synthetic implants, when compared to unmodified PET. Chitosan, which has been shown to have antimicrobial properties against *Staphylococcus aureus* and *Escherichia coli*, (Jou et al., 2007) has also been conjugated to PET in various ways to inhibit bacterial growth. Jung et al. (2007), using an electrospun chitosan-PET composite, observed significant bacteria inhibition of *S. aureus* and *Klebsiella pneumonia*. Another research group grafted chitosan onto PET and saw antimicrobial effects against *S. aureus* as well as *Pseudomonas aeruginosa.* (Jou et al., 2007)

Another problem incurred with hernia mesh materials is the risk for adhesion formations, especially with meshes used in the intraperitoneal cavity. (Brown and Finch, 2010) As discussed earlier, composite meshes have been developed to promote tissue in-growth on one side and reduce adhesion formation on the opposite side. Covidien has commercialized Parietex™ Composite, a PET mesh coated in collagen; however, researchers continue to develop additional coated PET meshes with the goal of limiting adhesion formations. Joseph et al. (2009) developed polyvinylidene (PVDF) coated PET and performed *in vitro* cytotoxicity assays to assess its biocompatibility. This development could be tested *in vivo* to observe adhesion formation, as PVDF has been utilized in other materials to reduce adhesions in hernia repair. (Brown and Finch, 2010)

Sandberg et al. (2009) proposed the use of mucins as biomaterial coatings and showed *in vitro* results of decreased adsorption of proinflammatory proteins to the surface, suggesting that the coatings could improve the biomaterial performance *in vivo*.

1.3 Gold Nanoparticles

In the last decade, use of gold nanoparticles (AuNP) in the medical world has drastically increased. AuNP have been used in biomedical applications such as targeted drug delivery, biosensors, cellular imaging, and cancer diagnostics, due to their unique size-related and optical properties, as well as their bioconjugation abilities. (Gu et al., 2009) Because of the earlier successes of AuNP in these applications, and their reported biocompatibility, (Gu et al., 2009; Castaneda et al., 2008; Connor et al., 2005; Hsu et al., 2007) recent research has focused on use of AuNP to enhance cell proliferation and antimicrobial properties of biomedical materials. (Castaneda et al., 2008; Hsu et al., 2007; Qu and Lü, 2009; Rai et al., 2010) However, while some literature reports AuNP to be biocompatible and non-cytotoxic, other studies have shown AuNP to be cytotoxic towards various cell lines. (Pernodet et al., 2006) It can be concluded that the particle diameter and concentration of AuNP, utilized in cell studies have significant effects on the biocompatibility results obtained from respective investigations.

In general, studies have shown that AuNP with smaller diameters (<15 nm) appear to have more toxic effects on cells than larger diameter AuNP. (Gu et al., 2009) This could potentially be because of the differences in cellular uptake of the nanoparticles by endocytosis; (Pernodet et al., 2006) the smaller particles are able to penetrate vesicles,

including the nucleus of the cell, whereas the larger diameter AuNP (~20 nm) possess different uptake kinetics and do not exhibit such adverse effects on the cells. (Gu et al., 2009) Because of the variability of results obtained regarding AuNP effects on cellular response, many studies have been conducted using larger AuNP in varying concentrations. Qu and Lü (2009) analyzed the cell viability of 20 nm AuNP at 10, 50, 100, 200, and 300 μM concentrations, and found that the nanoparticles did not decrease proliferation of human dermal fibroblast cells at any of the five concentrations tested. A similar study, performed using mice fibroblast cells, showed no adverse cell viability with AuNP concentrations up to 5 mM. (Castaneda et al., 2008) Hsu et al. (2007) conjugated AuNP, in four concentrations (17.4, 43.5, 65, and 174 ppm), to polyurethane (PU) to create PU-Au nanocomposites and performed cell attachment and proliferation studies as well as bacteria adhesion tests. Results from the cell viability studies with human gingival fibroblasts showed an increase in attachment and proliferation for all PU-Au nanocomposites in comparison to the original PU. Additionally, all concentrations of PU-Au nanocomposites exhibited significantly lower bacteria adhesion than the pure PU. (Hsu et al., 2007) Further antimicrobial properties of AuNP were shown by Rai et al. (2010) in a study using cefaclor bound AuNP. Although much of the antimicrobial activity must be contributed to the cefaclor, a second-generation antibiotic, results obtained for pure AuNP exposed to *S. aureus* and *E. coli* also exhibited a lower number of CFU than the control specimen. (Rai et al., 2010)

CHAPTER 2
INTRODUCTION TO RESEARCH

2.1 Significance of Research

Currently, implantation of a synthetic mesh patch is the most commonly used method for hernia repair; however, there has yet to be a product that performs consistently without complications *in vivo*. The significance of this research is the development of a more biocompatible PET mesh for potential use in hernia repair through chemical surface modifications and conjugations of AuNP. The proposed modifications should help to improve the long-term biocompatibility of PET while allowing the material to retain its flexibility and mechanical strength.

Explanted PET hernia meshes have shown signs of degradation when implanted for extended periods of time, resulting in physiochemical changes to the material.

Figure 1. Explanted PET mesh.

The susceptibility of PET to hydrolysis has been linked as a primary cause for these signs of degradation. (Grant and Ramshaw, 2010) Therefore, it is extremely important that chemical modification methods used on the PET mesh do not induce preemptive material degradation. It is difficult to assess the exact causes of PET mesh degradation *in vivo;* however, Costello et al. (2007b) analyzed explanted polypropylene hernia meshes and showed results of higher degradation with increased inflammatory response. This evidence suggests that a more biocompatible surface, which elicited less inflammatory response, could potentially assist in decreasing PET mesh degradation.

2.2 Research Objectives

The overall objective of this research was to improve the biocompatibility of PET mesh to potentially enhance long-term *in vivo* performance. Investigation of this project consisted of several studies within two main phases. The first phase concentrated on PET modification and characterization, while the second phase focused on biocompatibility testing of the modified PET through cell culture assays.

The first step of phase 1 was to perform a functionalization procedure to introduce carboxylic acid groups to the PET surface. Literature provided numerous options for surface functionalization and it was decided to use a chemical modification technique based on the desire for precise control of the polymer surface. Degradation of PET is also a major concern during modification processes; eventually, a carboxylation technique, which was shown by Muthuvijayan et al. (2009) to cause much less polymer surface degradation than hydrolysis or aminolysis, was selected and carried out on the

PET mesh. After characterization to assess introduction of appropriate functional groups, the PET meshes were cross-linked to functionalized AuNP to develop PET-AuNP scaffolds for use in biocompatibility testing. The PET-AuNP scaffolds were analyzed to confirm successful AuNP conjugation before being used in phase 2.

The second phase of this research consisted of analyzing the biocompatibility of the PET-AuNP scaffolds *in vitro.* Three individual cell culture studies were used to test the performance of the PET-AuNP scaffolds. Specifically, cell viability, reduction of reactive oxygen species, and antimicrobial properties of the PET-AuNP scaffolds were tested in the following experiments:

- Water soluble tetrazolium (WST-1) assay: used to qualitatively assess proliferation of cells exposed to PET and PET-AuNP scaffolds through absorbance correlation; simultaneously used to assess cytotoxic effects of AuNP
- OxiSelect™ ROS assay: used to measure the ability of AuNP, conjugated to PET, to reduce reactive oxygen species present in the cell culture
- Antimicrobial study: used to test the antimicrobial properties of AuNP by incubating PET and PET-AuNP scaffolds with bacteria and assessing colony forming units using plate counting techniques

Initial results from the three biocompatibility experiments of phase 2 were analyzed and used to optimize the concentrations of AuNP conjugated to PET. Material characterization and biocompatibility studies were then repeated using the new concentrations of PET-AuNP scaffolds.

CHAPTER 3
MODIFICATION AND CHARACTERIZATION OF PET-AUNP SCAFFOLDS

3.1 Overview

The objective of this study was to develop a gold nanoparticle (AuNP) conjugated polyethylene terephthalate (PET) mesh suitable for use in hernia repair. AuNP can be easily functionalized and cross-linked to functional groups on a substrate surface; however, pristine PET lacks active surface functional groups and therefore has to be modified to introduce active sites for conjugation. To begin this experiment, chemical modification methods were selected and performed on three types of PET mesh. Fourier transform infrared (FT-IR) spectroscopy was used to analyze the chemically modified PET and determine if appropriate functional groups had been introduced. In the second part of the modification procedure, AuNP were functionalized and cross-linked to functional groups on the PET surface using zero-length chemical cross-linkers. Images of the PET-AuNP scaffolds were taken using scanning electron microscopy (SEM) to confirm the presence, and abundance, of nanoparticles on the polymer surface. Energy dispersive spectroscopy (EDS) was used in conjunction with SEM to assess the composition of the surface conjugated particles. The aforementioned characterization methods were performed on each group of modified PET to assess the development of an AuNP conjugated PET mesh.

3.2 Materials and Methods

3.2.1 Chemicals and test substances

- PET hernia mesh
    - Parietex™ Flat Sheet Mesh, 3D weave – Covidien, Norwalk, CT
    - Parietex™ Flat Sheet Mesh, 2D weave – Covidien, Norwalk, CT
    - Mersilene™ Mesh – Ethicon, Somerville, NJ
- Hydrogen peroxide, 50 wt. % solution in water – Acros Organics, Thermo Fisher Scientific, Fair Lawn, NJ
- Cobalt (II) chloride, 97% – Sigma Aldrich, Saint Louis, MO
- Acetone, 99.5% – Acros Organics, Thermo Fisher Scientific, Fair Lawn, NJ
- Formaldehyde, 37% – Thermo Fisher Scientific, Fair Lawn, NJ
- Acetic acid, 99% – Sigma Aldrich, Saint Louis, MO
- Bromoacetic acid, 97% – Sigma Aldrich, Saint Louis, MO
- Sodium hydroxide – Thermo Fisher Scientific, Fair Lawn, NJ
- Gold colloids, 20 nm – Ted Pella, Redding, CA
- 2-mercaptoethylamine (MEA) – Sigma Aldrich, Saint Louis, MO
- 1-Ethyl-3-[3-dimethylaminopropyl]carbodiimide hydrochloride (EDC) – Sigma Aldrich, Saint Louis, MO
- *N*-hydroxysuccinimide (NHS) – Pierce, Thermo Fisher Scientific, Rockford, IL
- Phosphate buffered saline (PBS) – Sigma Aldrich, Saint Louis, MO

3.2.2 Chemical modification of PET

Three types of pristine PET hernia mesh were used for the material modification experiment: Parietex™ 3D mesh, Parietex™ 2D (flat) mesh, and Mersilene™ mesh. The PET mesh samples were cut into 1 cm x 1 cm squares, boiled in deionized water for 20 minutes, and dried thoroughly at room temperature prior to modification. All samples were stored in a desiccator until ready for use. Initially, two chemical modification protocols were selected: a hydrogen peroxide (H_2O_2) modification and a carboxylation technique.

H_2O_2 Protocol: The H_2O_2 modification procedure consisted of a seven day treatment of PET mesh with a 50% v/v solution of H_2O_2 in deionized water with 1.3 mg $CoCl_2$. The functionalization method was adapted from a protocol performed by Christenson et al. (2004), which used H_2O_2 and $CoCl_2$ to oxidize the surface of polyurethanes. The washed PET samples were immersed in 100 mL of the $H_2O_2/CoCl_2$ solution and placed on an orbital shaker table (150 rpm) for seven days. On the third and fifth days of the modification procedure fresh chemical solution was made and the PET samples were transferred to the new solution. After seven days, the samples were removed from the solution and dried thoroughly in a desiccator until ready for further testing.

Carboxylation Protocol: The carboxylation protocol used in this experiment was adapted from Muthuvijayan et al. (2009). This technique consists of a three step modification procedure which was shown by Muthuvijayan's group to cause less bulk degradation to PET than other, more common, methods of surface functionalization. (Muthuvijayan et al., 2009) First, a 50% v/v solution of acetone in deionized water was prepared. The

washed PET samples were immersed in 100 mL of the acetone solution and placed on an orbital shaker table (150 rpm) at room temperature for 24 hours. After 24 hours, the samples were removed from the acetone solution and dried thoroughly at room temperature inside a desiccator. For the second step of the carboxylation procedure, an 18.5% formaldehyde solution in 1 M acetic acid was prepared. The acetone-treated samples were shaken (150 rpm) in 100 mL of said solution for 4 hours at room temperature to hydroxylate the PET surface. Following the 4 hour treatment, samples were removed from the hydroxylation solution and dried at room temperature. The final step of the carboxylation procedure introduces carboxyl groups to the hydroxylated PET surface. A 100 mL solution of 1 M bromoacetic acid in 2 M sodium hydroxide was prepared and hydroxylated PET samples were immersed in the solution. The samples were shaken for 18 hours and then removed from the solution and dried thoroughly. The carboxylated PET mesh samples were stored in a desiccator until ready for characterization or future modification.

3.2.3 PET analysis using FT-IR

Surface properties of the PET mesh samples were analyzed using Fourier transform infrared (FT-IR) spectroscopy. Spectra were collected by a Nicolet 6700 FT-IR spectrometer (Thermo Fisher Scientific, Waltham, MA). A background scan of air was collected and subtracted from all sample readings to ensure the spectra were specific to the mesh composition. Initially, spectra of pristine PET samples were collected, providing a standard to compare the modified samples against. Final FT-IR scans were

taken for samples treated with each chemical modification protocol to assess the presence of surface functional groups. For the H_2O_2 modification procedure, only one modified scan was obtained; whereas for the carboxylation procedure, scans were taken after both the second and third steps to analyze the effect of each individual modification step.

3.2.4 AuNP conjugation

The surface functionalized PET mesh samples were conjugated to functionalized AuNP (f-AuNP) using a chemical cross-linking procedure. Each chemically modified PET sample was placed into a separate vial (15 mm diameter, 45 mm height) to carry out the AuNP conjugation. Functionalized AuNP were made using 20 nm gold colloid and 15 µM MEA. The thiol group provided preferential binding to the gold surface while leaving the amino group to be conjugated to the PET. EDC, a zero-length cross-linker, was used along with NHS to conjugate f-AuNP (amino groups) to reactive functional groups on the PET surface (carboxylate groups). The cross-linking solution was comprised of the following components: 2 mM EDC, 5 mM NHS, and 50% v/v acetone in 1x PBS. Each modified PET sample was incubated at room temperature with 1 mL cross-linking solution for 15 minutes to activate the surface functional groups. After 15 minutes, the cross-linking solution was removed and 0.25 mL f-AuNP was added to each vial. The vials were then placed on an orbital shaker table (75 rpm) for 24 hours to allow conjugation of AuNP to the PET surface. Following conjugation, the PET-AuNP scaffolds were washed in 1x PBS for 24 hours to remove un-conjugated particles. The PBS was then removed and the scaffolds were dried thoroughly at room temperature.

3.2.5 PET-AuNP scaffold analysis using SEM/EDS

Images of the PET-AuNP scaffolds along with surface composition analysis were obtained using scanning electron microscopy (SEM) and energy dispersive spectroscopy (EDS), respectively. Scanning electron micrographs were taken using a Quanta™ 600 scanning electron microscope with a field emission gun (FEG) system (FEI Company, Hillsboro, OR). Elemental analysis was performed by a Thermo Scientific NORAN System Six microanalysis system (Thermo Fisher Scientific, Waltham, MA), using point and shoot analysis to determine the composition of selected charged particles from the SEM image. All microscopy analysis of the PET-AuNP scaffolds was performed at the University of Missouri Electron Microscopy Core. SEM images and EDS data were obtained courtesy of Matthew Cozad.

3.3 Results and Discussion

3.3.1 Analysis of surface functionalization (FT-IR results)

FT-IR spectra were obtained for all three types of PET modified with the H_2O_2 modification procedure and the carboxylation technique, and compared to pristine PET scans to assess the introduction of functional groups. Spectra collected for the H_2O_2 modified PET are shown in Figures 2 – 4. It can be seen from the figures that the PET modified with the H_2O_2 protocol showed spectra very similar to that of pristine PET. This surface analysis indicates that functional groups were not introduced.

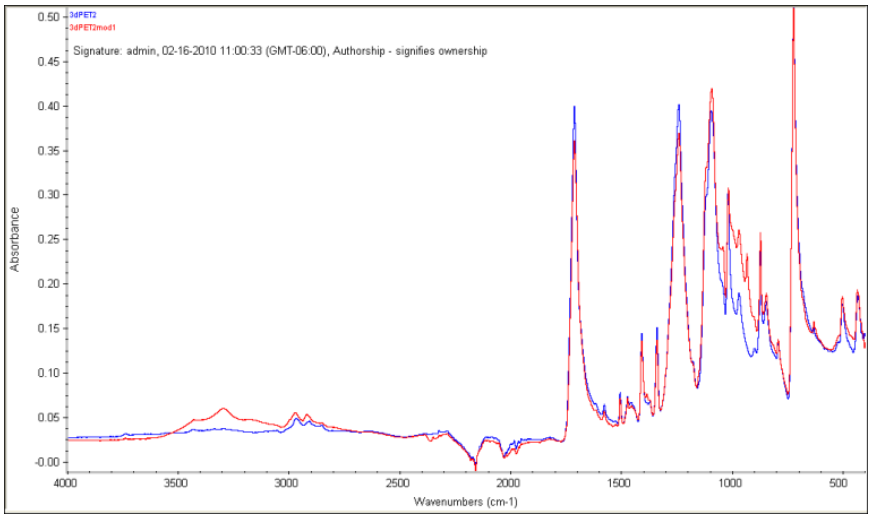

Figure 2. FT-IR spectra of Parietex™ 3D PET mesh: pristine (blue) and H_2O_2 modified (red).

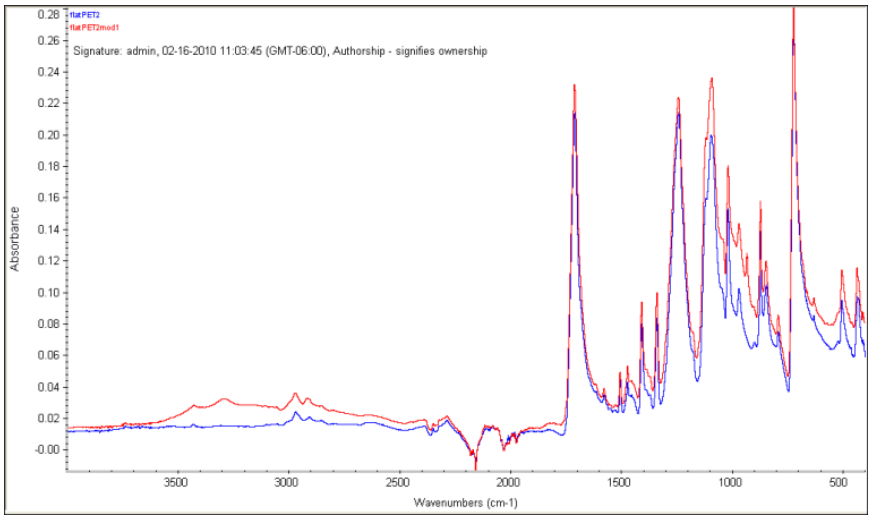

Figure 3. FT-IR spectra of Parietex™ 2D PET mesh: pristine (blue) and H_2O_2 modified (red).

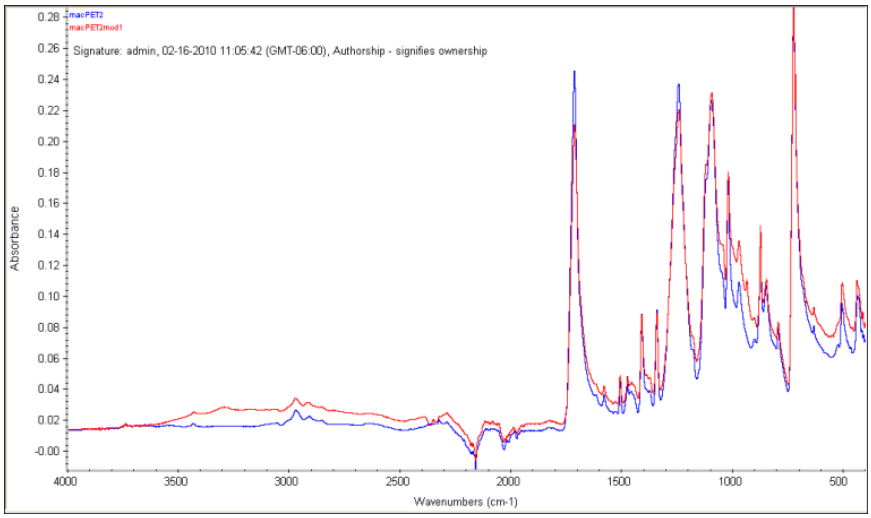

Figure 4. FT-IR spectra of Mersilene™ PET mesh: pristine (blue) and H_2O_2 modified (red).

Spectra obtained for the carboxylated PET samples are shown in Figures 5 – 7. The primary peaks of interest were the hydrogen-bonded O-H stretches, occurring at around 3000 – 3500 cm^{-1} for the hydroxylated PET and broadening to around 2500 – 3500 cm^{-1} after the carboxylation step. The former suggests the presence of alcohol groups whereas the latter suggests the addition of carboxylic acid functional groups. These observations from the FT-IR spectra are consistent with the theory presented by Muthuvijayan et al. (2009) in that the hydroxylation step of the protocol will add an O-H group to the PET surface, followed by the transformation of that group to a $COOH^-$ during the carboxylation step. It can also be observed from the spectra that the ester peak of the PET, occurring at around 1710 cm^{-1}, is broken during the carboxylation protocol, resulting in free surface functional groups.

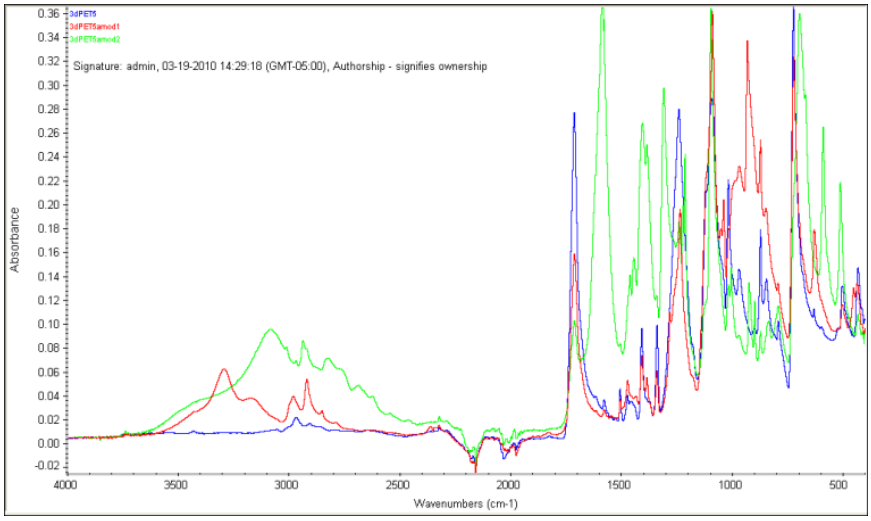

Figure 5. FT-IR spectra of Parietex™ 3D PET mesh: pristine (blue), hydroxylated (red), and carboxylated (green).

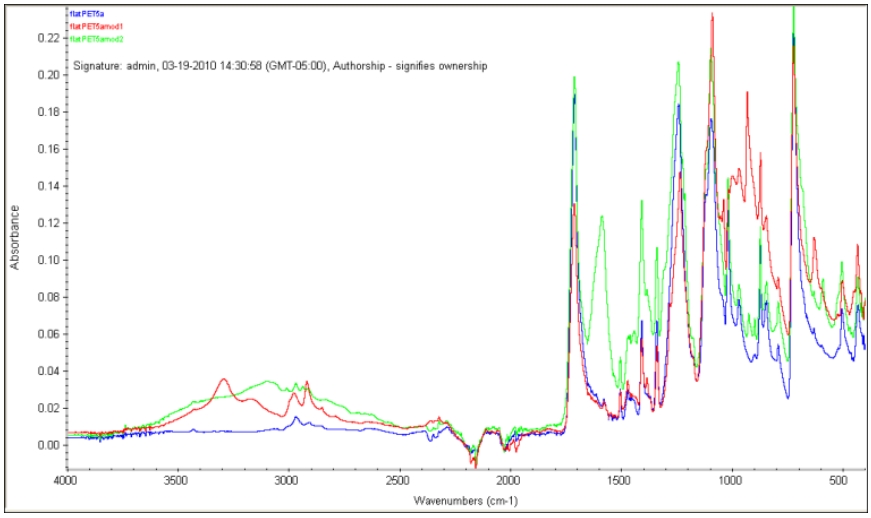

Figure 6. FT-IR spectra of Parietex™ 2D PET mesh: pristine (blue), hydroxylated (red), and carboxylated (green).

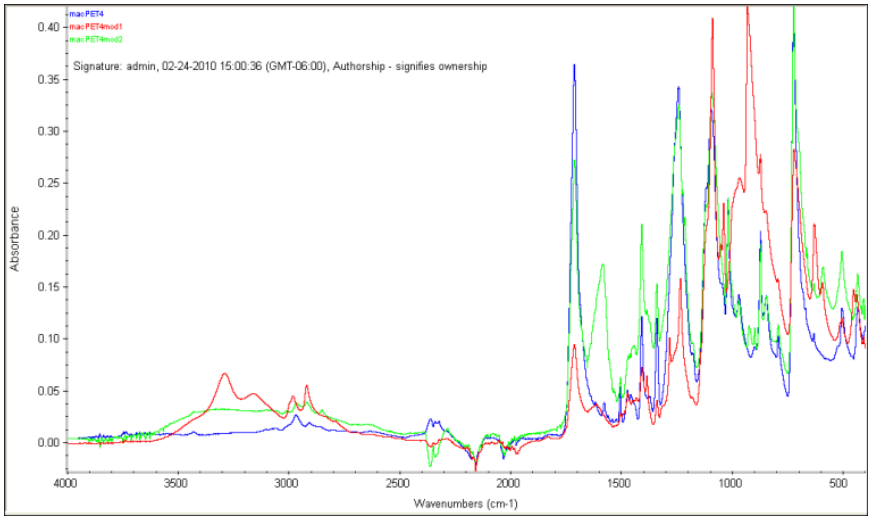

Figure 7. FT-IR spectra of Mersilene™ PET mesh: pristine (blue), hydroxylated (red), and carboxylated (green).

Overall, the FT-IR spectra indicated that the carboxylation technique was more effective in functionalizing the PET surface than the H_2O_2 modification procedure, as shown by the visually observable differences in spectra obtained for the pristine versus modified PET samples.

3.3.2 Analysis of surface functionalization (statistical analysis)

Although it can be seen from FT-IR spectra of carboxylated PET that Parietex™ 3D exhibits the largest carboxylic acid peaks, quantitative analysis was performed to assess the area under the peak from 2500 cm^{-1} to 3500 cm^{-1} for each of the three PET mesh types. The values obtained from the Omnic software were plotted for the three PET meshes to compare the peak areas (Figure 8). A one-way ANOVA found the means to be significantly different ($P < 0.05$) but a Tukey's multiple comparison post test did not find

significant differences when each of the experimental groups were compared. These results were expected since all three types of PET share the same composition; the only differences between them are their weaves and porosities. All statistical analysis was performed with GraphPad Prism® software, version 4.0.

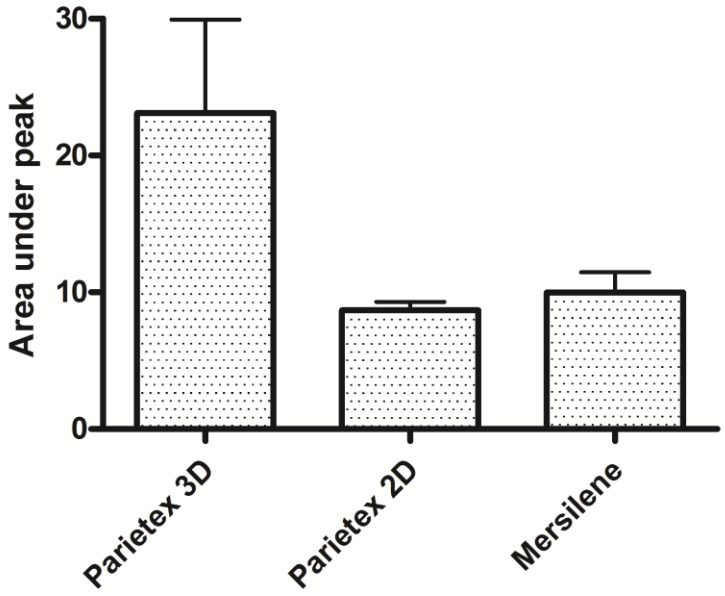

Figure 8. Average area under the carboxylic acid peak for the three PET meshes.

3.3.3 Analysis of AuNP conjugation

PET scaffolds modified with the carboxylation protocol and cross-linked with AuNP were analyzed using SEM and EDS to assess the presence of AuNP on the surface. Images obtained with SEM for the three types of PET-AuNP scaffolds are shown in Figures 9 – 11. The initial concentration of AuNP conjugated to the PET mesh was 1x, which correlates to $7x10^{11}$ particles per mL.

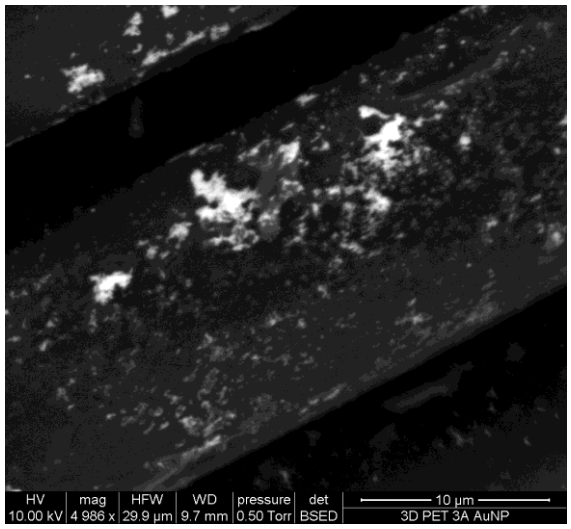

Figure 9. SEM image of Parietex™ 3D PET-AuNP scaffold.

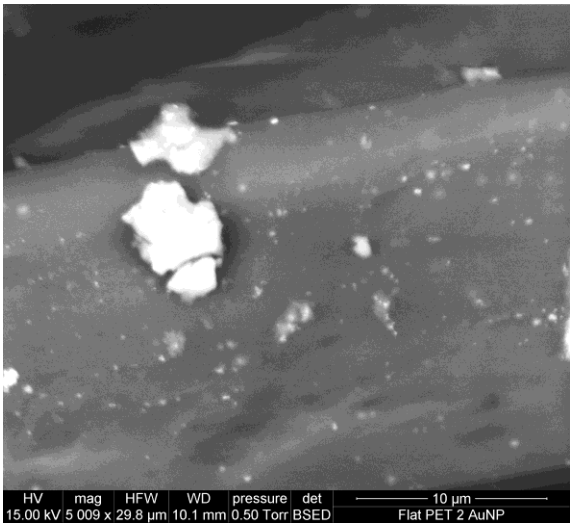

Figure 10. SEM image of Parietex™ 2D PET-AuNP scaffold.

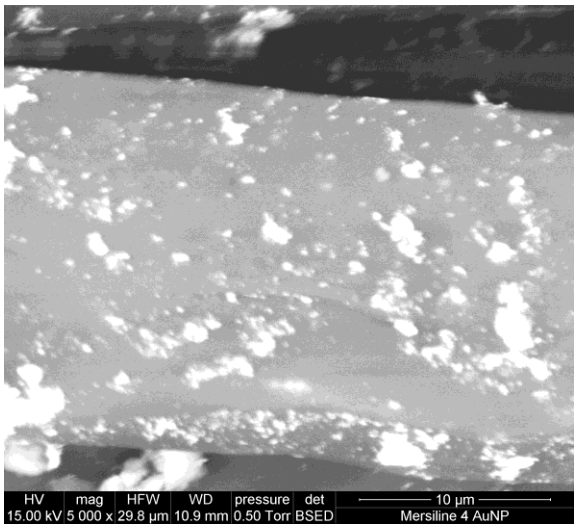

Figure 11. SEM image of Mersilene™ PET-AuNP scaffold.

It can been seen from the images of the PET-1xAuNP scaffolds that aggregates of charged particles have been conjugated to the surface of the PET mesh. To assess the composition of these particles, EDS point and shoot analysis was used. Presence of AuNP is suggested by peaks occurring around 2.14 keV in the EDS spectrum. Figures 12 and 13 show the elemental analysis of selected charged particles found to be gold on the PET surface. Additional figures are available in Appendix A.

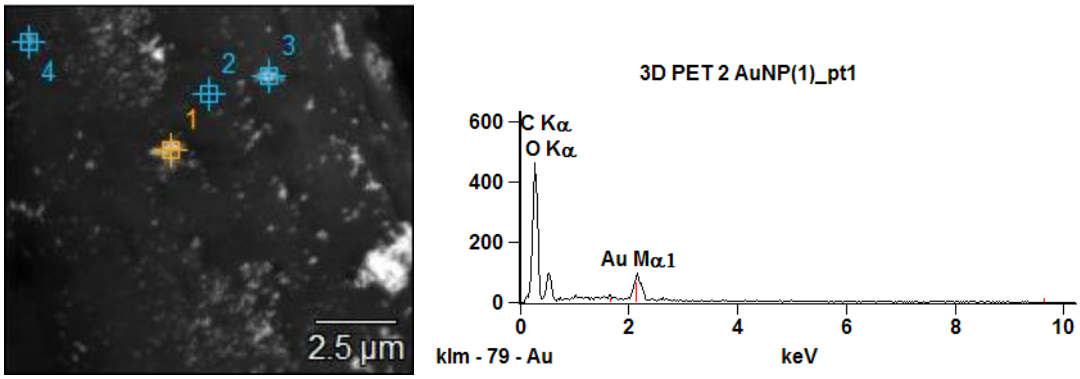

Figure 12. EDS analysis for point 1 selected on SEM image of Parietex™ 3D PET-1xAuNP.

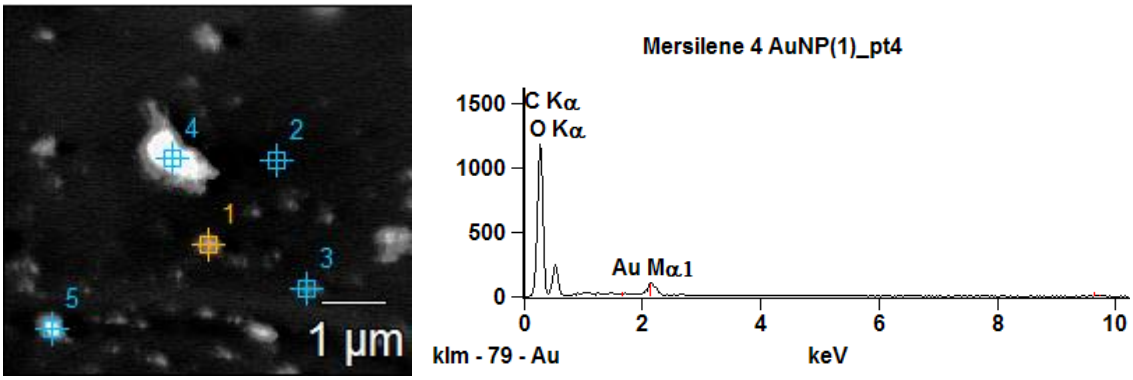

Figure 13. EDS analysis for point 4 selected on the SEM image of Mersilene™ PET-1xAuNP.

Initial results obtained from SEM images and EDS analysis showed that AuNP had successfully been cross-linked to the PET mesh surface. Images also indicated that aggregates of AuNP were formed during the cross-linking procedure and conjugated to the PET. Because of the overabundance of AuNP present on the PET surface, diluted solutions of AuNP were experimented with in additional cross-linking procedures. Diluted AuNP were made by adding distilled water to f-AuNP in the protocol presented in section 3.2.3. Further SEM images were taken to compare the distribution of AuNP on

the PET surface (Figures 14 – 18). EDS analysis was performed on the PET-0.5xAuNP scaffold and presence of gold was confirmed, as shown in Figure 19.

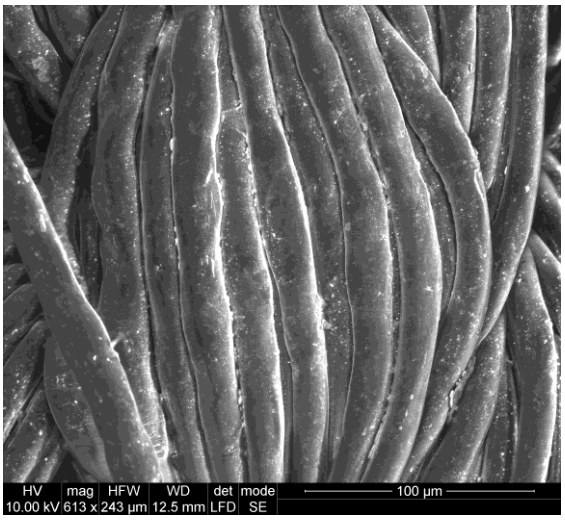

Figure 14. SEM image of PET-0.1xAuNP.

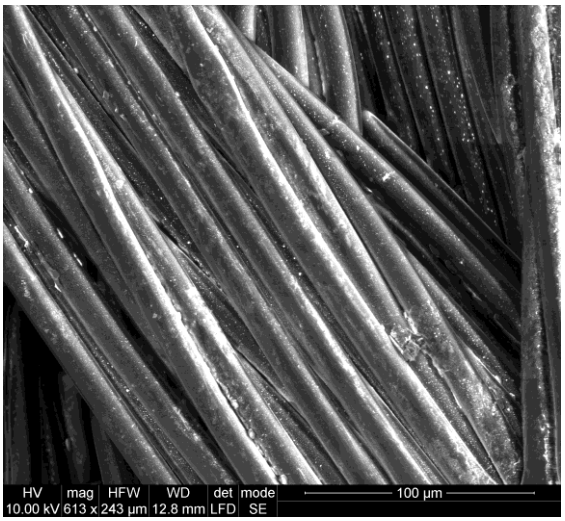

Figure 15. SEM image of PET-0.2xAuNP.

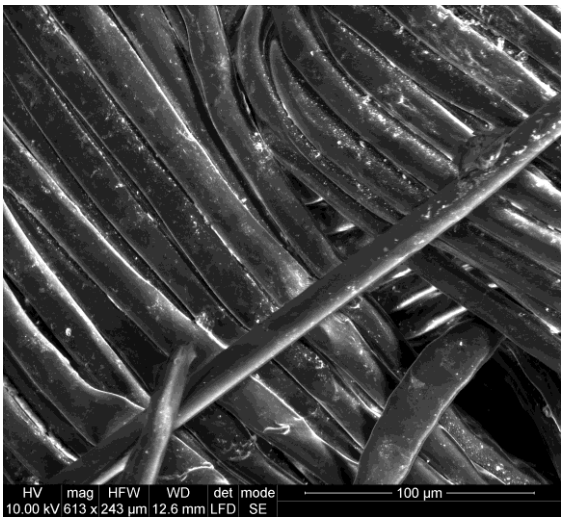

Figure 16. SEM image of PET-0.3xAuNP.

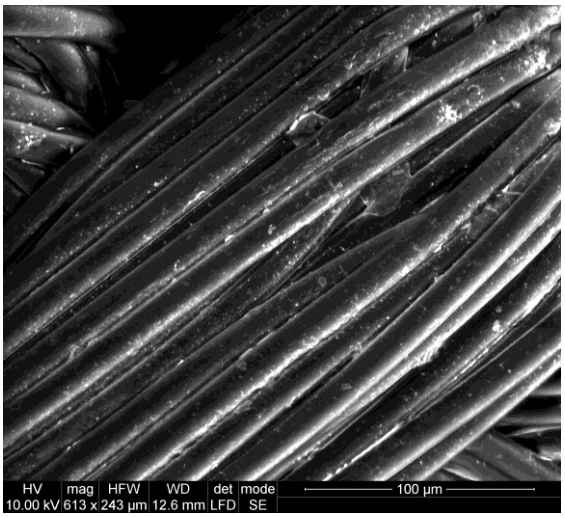

Figure 17. SEM image of PET-0.4xAuNP.

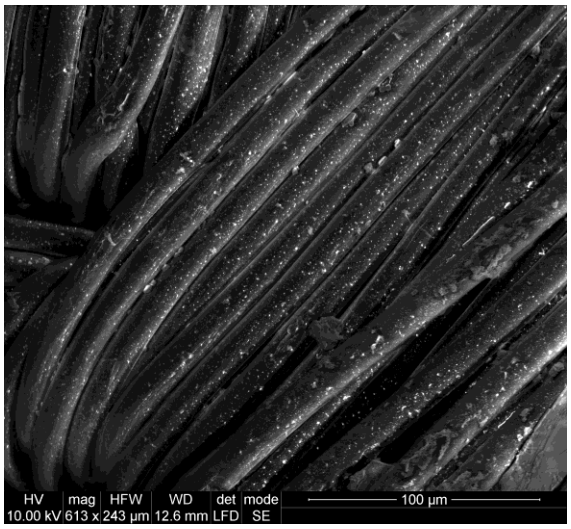

Figure 18. SEM image of PET-0.5xAuNP.

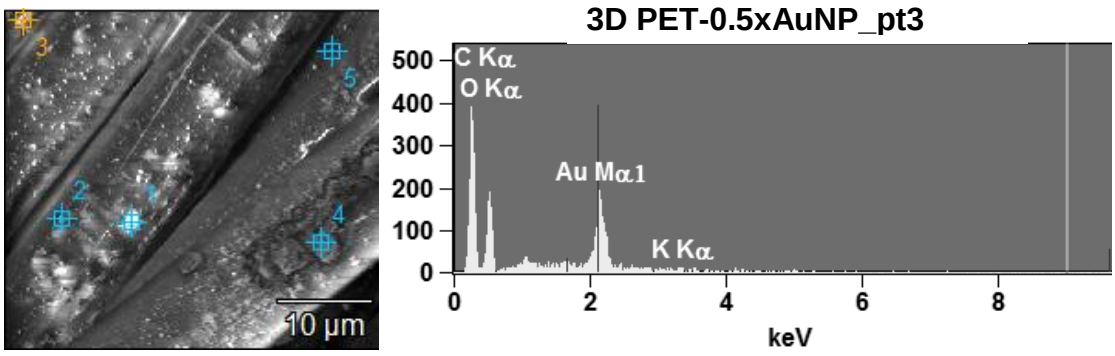

Figure 19. EDS analysis for point 3 selected on the SEM image of 3D PET-0.5xAuNP.

3.4 Conclusion

Results obtained from FT-IR spectra showed that PET mesh was able to be successfully functionalized by the carboxylation protocol, indicated by the introduction of carboxylic acid groups on the surface of the PET. All three types of PET mesh, Parietex™ 3D, Parietex™ 2D, and Mersilene™, were shown to have been functionalized;

however, peak area analysis of the FT-IR spectra for carboxylated samples found 3D PET to exhibit the most prominent carboxylic acid peaks, suggesting that it underwent the most effective modification. Because of this, 3D PET was selected as the mesh to be used in the remainder of this research investigation. The narrowing of the mesh types allowed for increased focus on optimizing the AuNP concentration throughout the remainder of the experiments.

Images obtained through SEM showed an abundance of charged particles on the surfaces of the PET-1xAuNP mesh. Point and shoot EDS analysis confirmed many of the particles as gold, indicating the success of AuNP conjugation to the surface of PET mesh. Visual observation of the SEM micrographs suggested that there were large amounts of aggregated gold present on the PET surface. Literature has shown that the concentration of AuNP on a polymer surface has a significant effect on *in vitro* cell response. (Hsu et al., 2007; Qu and Lü, 2009) Because of this, PET mesh was cross-linked with AuNP in various concentrations for use in biocompatibility testing. Additional SEM images were taken for diluted concentrations of AuNP and EDS data for the PET-0.5xAuNP confirmed the presence of gold. Although SEM and EDS data were not obtained for each concentration of AuNP on the PET-AuNP scaffolds, it can be assumed from the successes of the 0.5xAuNP and 1xAuNP conjugations that the same cross-linking protocol would be successful for other concentrations of AuNP.

CHAPTER 4
INVESTIGATION OF CELLULARITY OF PET-AUNP SCAFFOLDS

4.1 Overview

This investigation was performed to evaluate and analyze the response of cells to PET-AuNP scaffolds in comparison to pristine PET mesh (Parietex™ Flat Sheet Mesh, 3D weave). As discussed in Chapter 1, literature has provided contradicting evidence as to the toxicity of AuNP when implanted into the body and it has been shown that nanoparticle size, concentration, and immobilization play significant roles in determining cytotoxic effects. This investigation aimed to test the cellularity of PET conjugated to various concentrations of 20 nm AuNP in order to assess the PET-AuNP scaffolds' potential for use as an implantable biomaterial.

An unspecific, continuous line of murine fibroblast cells (L929) was selected to evaluate cell response to the PET-AuNP scaffolds. The cell line was chosen based on its demonstrated sensitivity in cytotoxicity testing. (Thonemann et al., 2002) Cell viability, proliferation, and cytotoxicity are commonly analyzed *in vitro* by measuring the metabolic activity of a population of cells by the reduction of a tetrazolium salt. In this experiment, a water soluble tetrazolium (WST-1) assay (Roche Diagnostics, Indianapolis, IN) was used to qualitatively measure and compare the cell responses of L929 fibroblasts grown in wells with the PET and PET-AuNP scaffolds. The principle of the WST-1 assay relies on the WST-1 reagent being reduced to a formazan dye by glycolic

production of NADPH in viable cells. Assays were conducted over three day and seven day time periods in order to observe potential differences in cell response to the scaffolds over time.

4.2 Materials and Methods

4.2.1 Chemicals and test substances

- L929 murine fibroblast cells (CCL 1) – American Type Culture Collection, Manassas, VA
- Culture medium – American Type Culture Collection, Manassas, VA
    - Eagle's Minimum Essential Medium
    - Horse Serum
    - Penicillin Streptomycin
- Dulbecco's Phosphate Buffered Saline (DPBS), 1x, without calcium and magnesium – American Type Culture Collection, Manassas, VA
- Trypan Blue – Sigma Aldrich, St. Louis, MO
- WST-1 Reagent – Roche Diagnostics, Indianapolis, IN

4.2.2 Preparation of cell culture for 3 day and 7 day studies

Before beginning the cultures for the three and seven day cell response studies, an aliquot of cells had to be subcultured from the stock L929 cell line. The L929 cells were continuously grown in plastic tissue culture flasks and subcultured when the flask was deemed sub confluent (i.e. when the cells reached about 80% confluency). To subculture cells for the WST-1 assay, all cell culture medium was removed from the sub confluent flask and the cell surface was washed with Dulbecco's phosphate buffered saline (DPBS). The adherent cells were then trypsinized and removed from the flask in 10 mL

of sterile culture medium. The dissociated cells were centrifuged in a 15 mL centrifuge tube and then re-suspended with 6 mL of sterile culture medium. All cell culture procedures were performed using aseptic technique; cells and solutions removed from the sterile biological hood were done so in closed containers and only opened when in a sterile environment.

Following re-suspension of the cells in culture medium, a small sample of cell suspension was removed from the centrifuge tube and used to calculate the cell concentration. Cells were stained with trypan blue and loaded into counting chambers of a hemocytometer. Viable cells were then counted to determine the concentration (cells/mL) of cells in the subcultured cell suspension. Appropriate ratios of cell suspension to sterile culture medium were calculated to result in the desired concentration of cells to be seeded in each WST-1 assay. For 3 day assays, cells were added to each well at a concentration of $3x10^4$ cells/mL. For 7 day assays, a concentration of $1.5x10^4$ cells/mL was used.

To begin the cell culture for the WST-1 assay, a 24-well plate was seeded with L929 cells in appropriate concentrations for the respective study. Each well received 1 mL of cell suspension/culture medium. The PET and PET-AuNP scaffolds were sterilized in a steam autoclave for 35 minutes at 121°C and then transported directly to the biological hood. The scaffolds were then added to each well of cells and the well plate was incubated at 37°C and 5% CO_2. For three day studies, the cells and scaffolds were incubated, undisturbed, for the duration of the assay; however, for seven day assays, the cell culture medium in each well had to be refreshed in order to keep the cells alive.

Culture medium was refreshed by carefully removing 0.5 mL of solution from each well, without disturbing the scaffold or cell surface, and pipetting 0.5 mL of fresh culture medium into the well. The culture medium refresh was performed on the third and fifth days of seven day studies.

4.2.3 Incubation of cells and scaffolds with WST-1

After the L929 cells were exposed to the PET and PET-AuNP scaffolds for the duration of their respective assay, WST-1 reagent was used to evaluate the cell response to each scaffold group. 0.5 mL of culture medium was carefully removed from each scaffold well to leave 0.5 mL of solution and the scaffold in each well. 50 µL of WST-1 reagent was then added to each scaffold well to create a 1:10 ratio of WST-1 to cell solution. A blank was also created by adding 0.5 mL of sterile cell culture medium and 50 µL of WST-1 reagent to an empty well. The well plate was then incubated at 37°C and 5% CO_2 until absorbance readings were taken.

4.2.4 Quantification of WST-1 assay

The viability of cells exposed to the PET and PET-AuNP scaffolds was quantified by measuring the absorbance of the formazan dye in each scaffold well. Absorbance readings were taken after one and two hours of incubation with the WST-1 reagent. To measure the absorbance, 100 µL of solution from each scaffold well and the blank was removed and placed into a corresponding well in a 96-well microplate. The microplate was then read by a Bio-Rad Model 680 Microplate Reader (Bio-Rad Laboratories,

Hercules, CA) and data was interpreted by Microplate Manager Software, version 5.2.1. The blank absorbance was subtracted from the total absorbance for each well to account for any absorbance encountered from the solution not attributed to cellularity.

4.2.5 Statistical analysis

All experimental groups were represented by at least four samples in each WST-1 assay to provide a sufficient mean value and calculate standard deviations within the group. All statistical analysis was performed using GraphPad Prism® software, version 4.0. A one-way analysis of variance (ANOVA) test with a 95% confidence interval was performed to determine significant differences between the experimental means. For experiments with a P-value less than 0.05, a post-test, Tukey's multiple comparison test, was performed to compare each individual group within the experiment.

4.3 Results and Discussion

4.3.1 WST-1 3 day assay

To initially observe the L929 cell response to the PET and PET-AuNP scaffolds, a 3 day WST-1 assay was performed. Pristine PET mesh was used as the control group and PET-0.5xAuNP and PET-1xAuNP scaffolds were used as experimental test groups. Absorbance readings were taken after one and two hour incubations of the cells with WST-1 reagent and results are shown in Figures 20 and 21. At incubation times longer than two hours, the absorbance became too high for the microplate reader and no values were able to be obtained. After one hour of incubation the absorbance values were

highest for the PET (control), suggesting that cells may be more viable when exposed to pristine PET than when exposed to PET-AuNP scaffolds. However, when readings were taken after two hours, the PET-1xAuNP exhibited the highest cellularity. One-way ANOVAs were performed for both incubation times and neither set of experimental data was shown to be significantly different.

It was hypothesized that AuNP would have a more definitive effect on cellularity if the cells were in direct contact with the scaffolds for a longer period of time. Therefore, it was decided to extend the cell culture for the WST-1 assay from a 3 day study to a 7 day study.

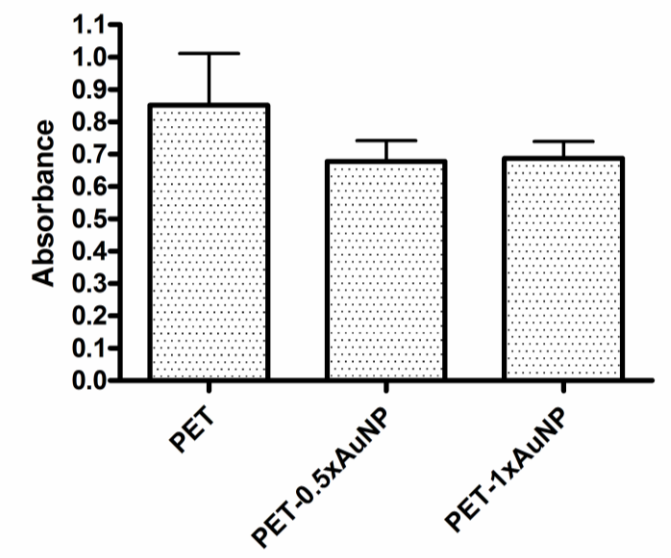

Figure 20. Absorbance values from a 3 day WST-1 assay incubated with WST-1 reagent for 1 hour

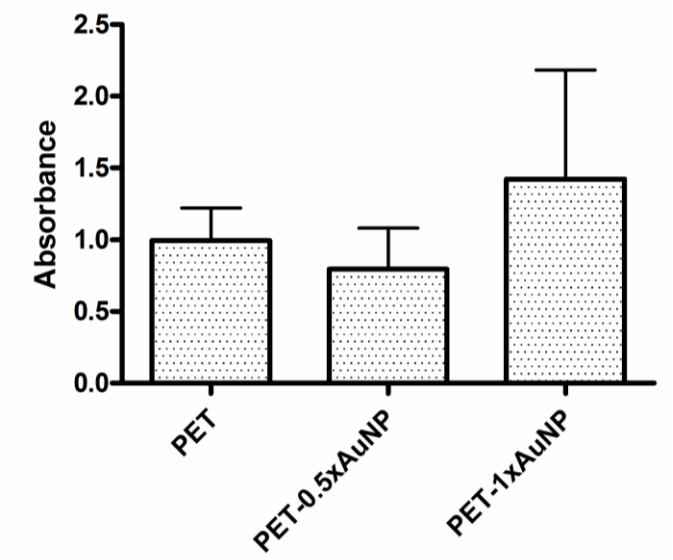

Figure 21. Absorbance values from a 3 day WST-1 assay incubated with WST-1 reagent for 2 hours.

4.3.2 WST-1 7 day assay

To extend the cell culture for the WST-1 assay from 3 days to 7 days, adjustments were made to the initial cell concentration at which the assays were seeded to allow for longer duration of cell growth. Pristine PET remained as the control group and three groups of experimental scaffolds were used: PET-0.25xAuNP, PET-0.5xAuNP, and PET-1xAuNP. Absorbance measurements were taken after one and two hour incubations of the scaffolds and medium with the WST-1 reagent and are shown in Figures 22 and 23.

The absorbance readings from the one hour incubation showed PET-1xAuNP scaffolds to exhibit the highest absorbance, pristine PET to be in the middle range, and PET-0.25xAuNP and PET-0.5xAuNP scaffolds to have the lowest absorbance. This trend is similar to what was observed with the two hour incubation of the 3 day assay discussed in section 4.3.1. A one-way ANOVA was performed for the results and the difference between the experimental means was found to be significant with a 95%

confidence interval. However, Tukey's multiple comparison test found the PET-1xAuNP scaffolds to be significantly different from the PET-0.25xAuNP and PET-0.5xAuNP scaffolds, but not from the pristine PET. P-values from the post-test are listed in Table 3.

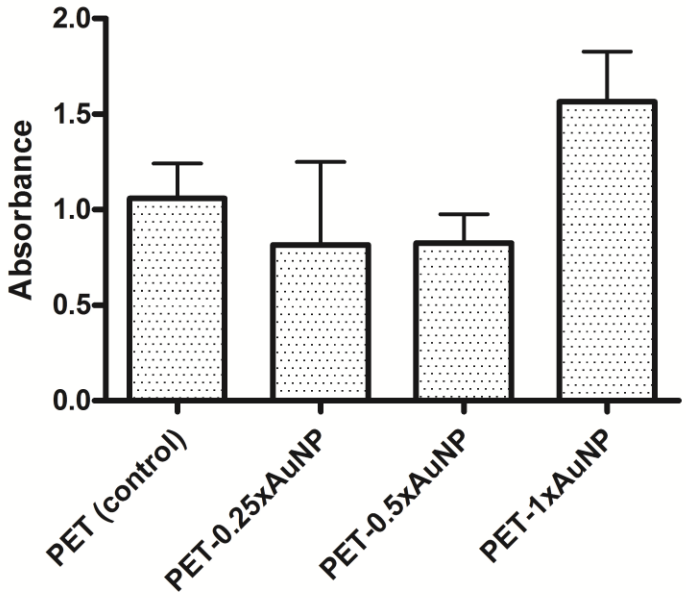

Figure 22. Absorbance readings after 1 hour incubation of the 7 day WST-1 assay.

Table 3. P-values for ANOVA of 1 hour WST-1 assay.

PET (control) vs. PET-0.25xAuNP	P > 0.05
PET (control) vs. PET-0.5xAuNP	P > 0.05
PET (control) vs. PET-1xAuNP	P > 0.05
PET-0.25xAuNP vs. PET-0.5xAuNP	P > 0.05
PET-0.25xAuNP vs. PET-1xAuNP	P < 0.05
PET-0.5xAuNP vs. PET-1xAuNP	P < 0.05

After two hours of incubation with the WST-1 reagent, the absorbance values for all the scaffold groups followed the same general trend as in the one hour incubation;

however, the gap had widened between the PET-1xAuNP scaffolds and the other three groups of scaffolds. A one-way ANOVA showed the means to be significantly different with a 99% confidence interval. Tukey's multiple comparison test showed the absorbance for the PET-1xAuNP scaffold wells to be significantly different when compared against the other groups as individuals. These results suggest that L929 cells directly exposed to PET-1xAuNP *exhibit enhanced cell viability and proliferation over those exposed to pristine PET mesh*. The relatively similar absorbance values of the PET-0.25xAuNP and PET-0.5xAuNP to the pristine PET also showed that AuNP, when conjugated to PET mesh, did not elicit a cytotoxic response.

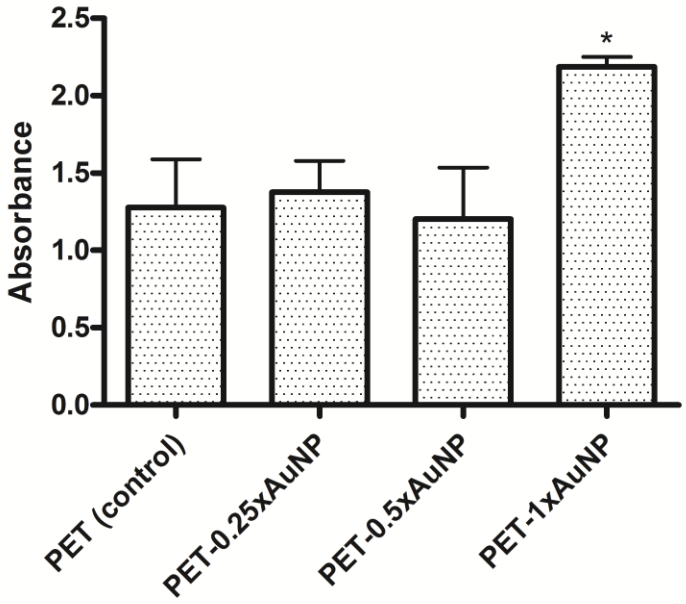

Figure 23. Absorbance values after a 2 hour incubation of the 7 day WST-1 assay. *Significant increase over each group (P<0.01 for PET-1xAuNP vs. PET)

Table 4. P-values for ANOVA of 2 hour incubation.

PET (control) vs. PET-0.25xAuNP	$P > 0.05$
PET (control) vs. PET-0.5xAuNP	$P > 0.05$
PET (control) vs. PET-1xAuNP	$P < 0.01$
PET-0.25xAuNP vs. PET-0.5xAuNP	$P > 0.05$
PET-0.25xAuNP vs. PET-1xAuNP	$P < 0.01$
PET-0.5xAuNP vs. PET-1xAuNP	$P < 0.001$

4.4 Conclusion

The WST-1 assays performed in this investigation of L929 cell response to PET-AuNP scaffolds in varying concentrations showed evidence that use of AuNP conjugated to PET mesh could enhance the viability and proliferation of surrounding cells. The results also showed that the AuNP did not seem to have any significant cytotoxic effects on the cells during the 3 or 7 day exposures. The cell culture exposed to the scaffolds for 7 days resulted in more definitive results than the assay cultured for only 3 days, although a similar trend was seen for each of the lengths of assays. All repetitions of assays within this investigation followed this trend, indicating the reproducibility of the study.

CHAPTER 5
INVESTIGATION OF REACTIVE OXYGEN SPECIES REDUCTION BY PET-AUNP SCAFFOLD

5.1 Overview

5.1.1 Significance of reactive oxygen species

The objective of this study was to investigate the potential for AuNP conjugated to PET mesh to act as scavengers of reactive oxygen species (ROS). ROS, also referred to as free radicals, are molecules which lack a full set of electrons thus causing them to be unstable and highly reactive. While a limited amount of ROS are present in and vital to biological systems, excess amounts can be produced by inflammation and infection, potentially leading to cell damage and destruction of the surrounding biological tissue. (Elswaifi et al., 2009) As discussed in Chapter 1, there is currently not an available hernia mesh that does not elicit some type of foreign body response. The inflammatory reaction incurred as a result of hernia mesh implantation has been shown to increase the oxidation, and therefore degradation, of synthetic mesh *in vivo*. (Costello et al., 2007b) It is plausible that increased production of ROS, as a byproduct of the inflammatory response, correlates to the oxidation of implanted meshes. With inflammation and infection being common occurrences in hernia repair, a mesh with ROS reducing capabilities would result in a vast improvement in the biocompatibility of synthetic hernia meshes. The use of nanoparticles as antioxidants has been researched and potential has been shown for their use in nanomedicine. (Elswaifi et al., 2009) This investigation aims to assess the

ability of PET-AuNP scaffolds to act as antioxidants and significantly reduce ROS through use of *in vitro* cell culture assays.

5.1.2 OxiSelect™ Intracellular ROS Assay Kit

The OxiSelect™ Intracellular ROS Assay Kit (Cell Biolabs, San Diego, CA) was used in this study to measure the ROS activity within cells when exposed to PET and PET-AuNP scaffolds. The ROS assay utilizes 2'-7'-Dichlorodihydrofluorescin diacetate (DCFH-DA), a cell-permeable fluorogenic probe, to carry out the mechanism of quantifying the ROS activity. Briefly, the DCFH-DA penetrates the cell membranes and is then transformed by cellular esterase to non-fluorescent 2'-7'-Dichlorodihydrofluorescin (DCFH). In the presence of ROS, DCFH oxidizes to fluorescent 2'-7'-Dichlorodihydrofluorescin (DCF) and its fluorescence intensity can be read by a spectrofluorometer. The principle of this assay is that an increased amount of ROS will yield an increased amount of DCF, thus resulting in higher fluorescence intensity which can then be correlated to the amount of ROS present in the sample. A DCF standard curve is utilized to establish a quantitative relationship between the measured fluorescence intensities and the amount of ROS activity.

5.2 Materials and Methods

5.2.1 Chemicals and test substances

- OxiSelect™ ROS Assay Kit – Cell Biolabs, San Diego, CA
    - 20x DCFH-DA – 20 mM solution in methanol
    - DCF Standard – 1 mM solution in dimethyl sulfoxide

    - 2x Cell Lysis Buffer
- Culture Medium – American Type Culture Collection, Manassas, VA
    - Eagle's Minimum Essential Medium
    - Horse Serum
    - Penicillin Streptomycin
- Dulbecco's Phosphate Buffered Saline (1x, without calcium and magnesium) – American Type Culture Collection, Manassas, VA
- L929 Cell Line – American Type Culture Collection, Manassas, VA

5.2.2 Preparation of cell culture for ROS assays

Prior to the start of the ROS assay L929 murine fibroblast cells were subcultured and seeded in a 24-well plate at a concentration of $1x10^5$ cells/mL. The subculture, counting, and seeding procedures were performed following the same protocol as described in Chapter 4. Each well contained cells suspended in 1 mL of sterile culture medium. The well plate of cells was then incubated in an air atmosphere at 37°C and 5% CO_2 for 24 hours. After the cell culture was allowed to proliferate for 24 hours, all culture medium was removed and discarded. Each experimental well was rinsed three times with DPBS. The 20x DCFH-DA was diluted with DPBS to yield 1x DCFH-DA/DPBS and 0.15 mL was added to each experimental well. The well plate was then incubated for 1 hour at 37°C and 5% CO_2. Following the incubation, the 1x DCFH-DA/DPBS was removed and each well was rinsed with DPBS. All PET and PET-AuNP scaffolds were sterilized with a steam autoclave at 121°C for 35 minutes and transferred directly to the sterile biological hood. The scaffolds were then added to the well plate, covered with 0.5 mL DPBS, and incubated at 37°C and 5% CO_2 for 12 hours.

5.2.3 Quantification of ROS reduction by PET-AuNP scaffolds

The ROS assay was terminated after the 12 hour incubation of the scaffolds by adding 0.5 mL of cell lysis buffer to each well and incubating for 5 minutes. The assay plate was then removed from the incubator and 0.25 mL of solution from each well was transferred to separate 1.5 mL cuvettes. Fluorescence spectroscopy was used to measure the fluorescence intensity of each cuvette, which directly correlates to ROS activity of each sample. All fluorescence measurements were taken with a FluoroMax®-3 Spectrofluorometer (Horiba Jobin Yvon, Edison, NJ). The excitation and emission wavelengths used were 480 nm and 530 nm, respectively. Fluorescence intensities were analyzed using FluorEssence™ software, version 2.1.6 (Horiba Jobin Yvon, Edison, NJ).

5.2.4 Preparation of DCF standard curve

In order to quantitatively correlate the measured fluorescence intensities to the amount of ROS present, a curve using the stock DCF reagent was prepared. The DCF standard solution was series diluted in DPBS to yield concentrations ranging from 0 to 10,000 nM. 0.125 mL of each diluted standard was mixed with 0.125 mL of 2x cell lysis buffer and transferred to individual 1.5 mL cuvettes. The fluorescence was then measured using the same methods and equipment as in section 5.2.3.

5.2.5 Statistical analysis

All experimental groups were represented by at least four samples in each ROS assay to establish a sufficient mean value and to determine standard deviations within

each group. All statistical analysis was performed using GraphPad Prism® software, version 4.0. The correlation between fluorescence intensity and DCF concentration for each sample was determined by linear regression analysis using the data obtained from the DCF standard curve. DCF concentrations for the experimental group samples were obtained by interpolation of the DCF standard curve fit to a straight line. Significant differences between the means of the experimental groups were determined by a one-way analysis of variance (ANOVA) with a 95% confidence interval. For experiments found to be significantly different, Tukey's multiple comparison test was performed as a post-test to establish P-values for and compare each individual group within the experiment.

5.3 Results and Discussion

5.3.1 ROS Assay with AuNP concentrations of 0.25x, 0.5x, and 1x

To initially assess the ability of PET-AuNP scaffolds to act as antioxidants, four groups of scaffolds were tested: pristine PET, PET-0.25xAuNP, PET-0.5xAuNP, and PET-1xAuNP. Pristine PET served as the control group and the PET-AuNP scaffolds, in varying concentrations, served as the experimental groups. As literature has shown, the concentration of AuNP has a significant impact on cell response, therefore a relatively broad range of AuNP concentrations were used initially in order to establish an idea of the ROS reducing capabilities of the PET-AuNP scaffolds.

Initial fluorescence intensity values from the four scaffold groups are shown in Figure 24. The mean value for each group was plotted with the error bar representing the standard deviation between repetitions within an individual group. It can be seen from

the graph that there was substantial variation in the control group as well as in the PET-0.5xAuNP and PET-1xAuNP scaffold groups. The PET-0.25xAuNP scaffolds showed much less deviation than any other group and also gave the lowest fluorescence intensities; however, a one-way ANOVA showed no significant difference between the means of the scaffold groups.

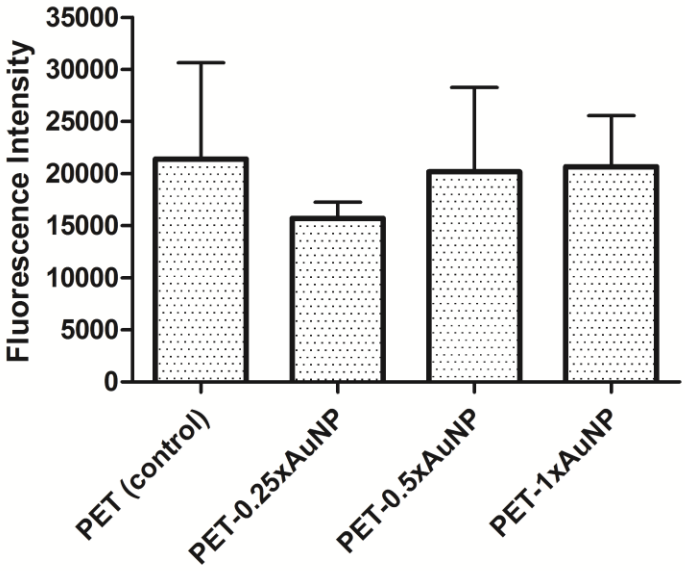

Figure 24. Mean fluorescence intensities for each scaffold group in the ROS assay.

The plot of the DCF standard curve from the series diluted stock DCF solution is shown in Figure 25. Fluorescence intensity values from the curve were analyzed using linear regression to obtain a quantitative correlation between measured fluorescence and DCF concentration. The goodness of fit analysis resulted in an r^2 value of 0.9952. The raw fluorescence intensities from each scaffold were then interpolated based on the standard curve and the corresponding DCF concentrations of each scaffold group were

calculated. As shown in Figure 26, the mean DCF concentrations for the four groups followed a trend similar to that of the fluorescence, which was to be expected. Likewise, a one-way ANOVA showed no significant differences between the scaffold group means.

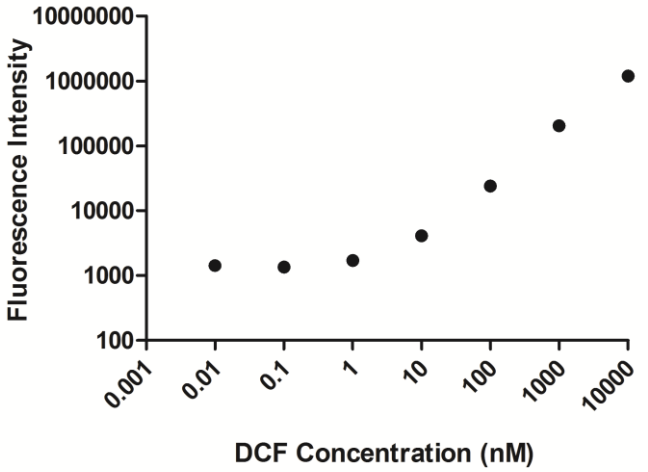

Figure 25. DCF standard curve for the series diluted stock DCF.

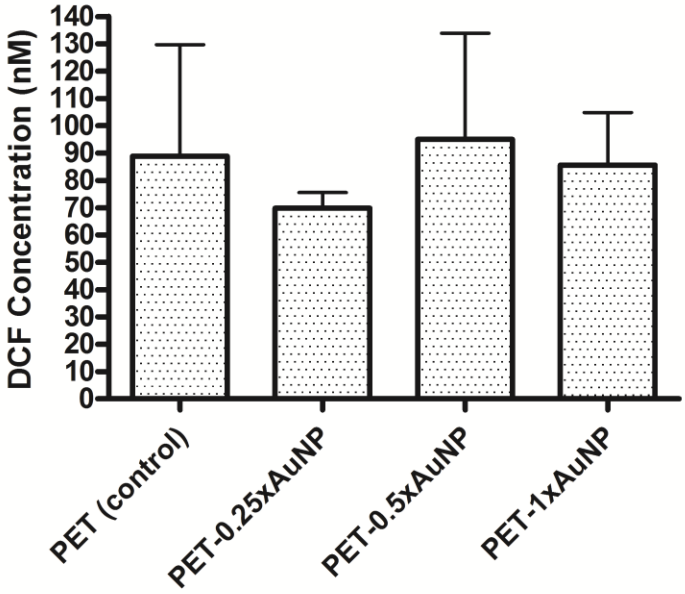

Figure 26. Interpolated DCF concentrations for each scaffold group.

Although statistical analysis did not show the PET-0.25xAuNP scaffolds to act as significant free radical scavengers, DCF concentrations for each of the repetitions of the PET-0.25xAuNP scaffolds were consistently lower than values for the other groups, suggesting that AuNP in low concentrations may have greater antioxidant potential. This information was utilized to assess parameters for the modification of PET for scaffolds to be used in future assays.

5.3.2 ROS Assay with AuNP concentrations of 0.1x, 0.2x, 0.3x, 0.4x, and 0.5x

Based on the results discussed in section 5.3.1, it was hypothesized that AuNP in low concentrations have greater potential to act as free radical scavengers than those in high concentrations. Therefore, the ROS assay was repeated using new experimental scaffold groups. Pristine PET remained as the control group, whereas the experimental groups consisted of PET-0.1xAuNP, PET-0.2xAuNP, PET-0.3xAuNP, PET-0.4xAuNP, and PET-0.5xAuNP scaffolds.

Fluorescence intensities for each of the scaffold groups were obtained and the means plotted in Figure 27. The mean intensities for each of the experimental groups were shown to be lower than those of the control PET group, suggesting that low concentrations of AuNP may have potential to act as antioxidants, as hypothesized. A one-way ANOVA with a 95% confidence interval showed the means of the scaffold groups to be significantly different. Tukey's multiple comparison test was performed as a post-test and found the PET-0.1xAuNP and PET-0.3xAuNP scaffolds to have significantly less fluorescence intensity than the PET (control).

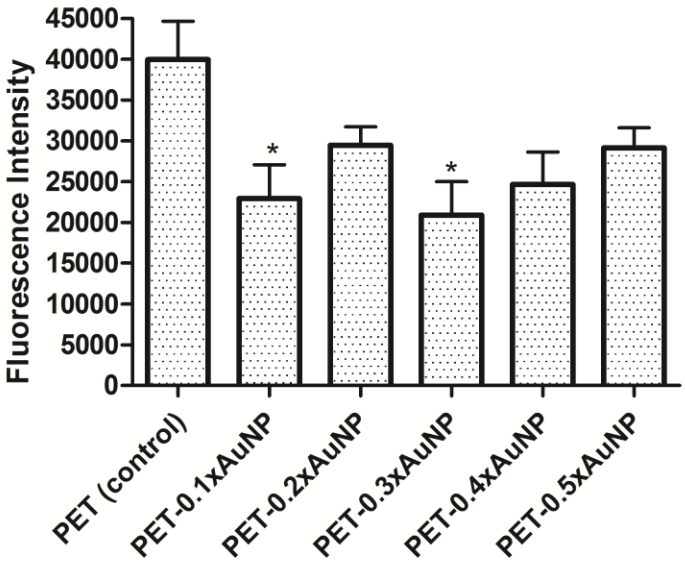

Figure 27. Mean fluorescence intensities for each scaffold group.

***Significant decrease compared to control (P<0.05)**

A DCF standard curve was prepared from a series dilution of the stock DCF standard solution and the measured fluorescence was plotted in Figure 28. Linear regression analysis resulted in an r^2 value of 0.9934 and the scaffolds' fluorescence intensities were interpolated into DCF concentrations based on the standard curve. As expected, the interpolated DCF concentrations for each scaffold group followed the same trend as the corresponding fluorescence intensities. A one-way ANOVA showed a significant difference between the means of the DCF concentrations with a P-value of 0.0203. Tukey's multiple comparison test showed the PET-0.1xAuNP and PET-0.3xAuNP scaffold groups to have significantly lower DCF concentrations than the control PET group.

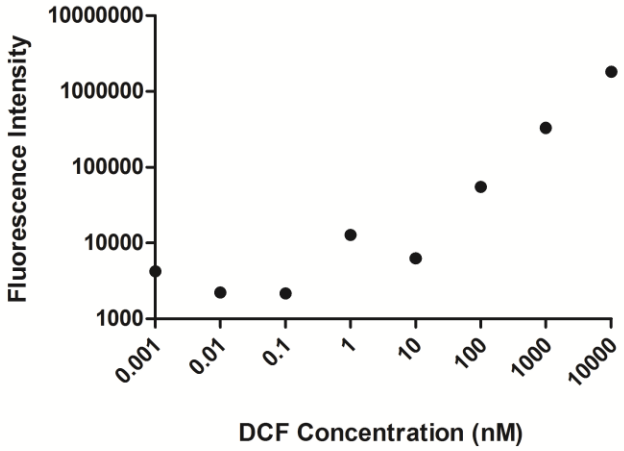

Figure 28. DCF standard curve for series diluted stock DCF solution.

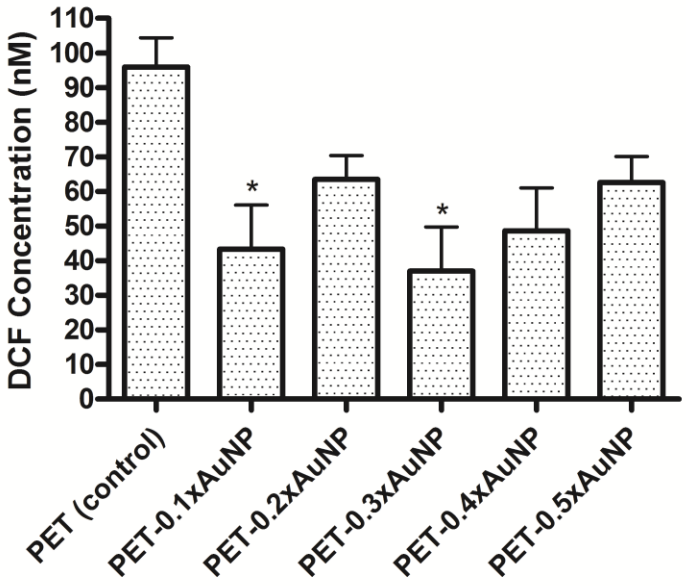

Figure 29. Interpolated DCF concentrations for each scaffold group.

***Significant decrease (P<0.05)**

Table 5. P-values for ANOVA of DCF concentration.

PET (control) vs. PET-0.1xAuNP	$P < 0.05$
PET (control) vs. PET-0.2xAuNP	$P > 0.05$
PET (control) vs. PET-0.3xAuNP	$P < 0.05$
PET (control) vs. PET-0.4xAuNP	$P > 0.05$
PET (control) vs. PET-0.5xAuNP	$P > 0.05$
PET-0.1xAuNP vs. PET-0.2xAuNP	$P > 0.05$
PET-0.1xAuNP vs. PET-0.3xAuNP	$P > 0.05$
PET-0.1xAuNP vs. PET-0.4xAuNP	$P > 0.05$
PET-0.1xAuNP vs. PET-0.5xAuNP	$P > 0.05$
PET-0.2xAuNP vs. PET-0.3xAuNP	$P > 0.05$
PET-0.2xAuNP vs. PET-0.4xAuNP	$P > 0.05$
PET-0.2xAuNP vs. PET-0.5xAuNP	$P > 0.05$
PET-0.3xAuNP vs. PET-0.4xAuNP	$P > 0.05$
PET-0.3xAuNP vs. PET-0.5xAuNP	$P > 0.05$
PET-0.4xAuNP vs. PET-0.5xAuNP	$P > 0.05$

Results obtained from low concentration range ROS assay, although significant, failed to demonstrate a distinct trend. The reduction of ROS by the PET-0.1xAuNP and PET-0.3xAuNP scaffolds supported the hypothesis of lower AuNP concentrations having greater antioxidant properties than higher AuNP concentrations; however, the PET-0.2xAuNP showed DCF concentration values higher than any other experimental scaffold group.

5.4 Conclusion

The ROS assays performed in the investigation of antioxidant properties of AuNP conjugated to PET mesh showed promising, but inconsistent, results. The initial assays using the broad range of AuNP concentrations on the PET scaffolds did not show any

significant differences in ROS activity and the data was primarily used to funnel the focus of the subsequent assays. The following set of assays, using the range of lower concentrations of AuNP conjugated to the PET mesh, demonstrated the PET-AuNP scaffolds' abilities to significantly reduce reactive oxygen species but was unable to provide an ideal concentration range. This result could possibly be contributed to AuNP aggregation during conjugation, causing the concentration to behave as higher than the expected 0.2xAuNP. A more specific determination of the cause for this scaffold group to behave differently than other "low AuNP concentration" scaffolds could possibly be investigated through extensive surface analysis of each sample scaffold.

Statistical analysis used to compare individual scaffold groups, Tukey's multiple comparison test, found significant differences ($P<0.05$) only for the PET (control) vs. PET-0.1xAuNP and the PET (control) vs. PET-0.3xAuNP. These results indicate that the differences in DCF concentration between each group of PET-AuNP scaffolds was somewhat negligible and could support the hypothesis that significantly reduced ROS activity could be observed for the other PET-AuNP scaffolds if longer incubation times were implemented. As seen in the cytotoxicity test results in Chapter 4, the duration in which the AuNP were allowed to interact with the cells had a significant impact on the outcome of the results.

CHAPTER 6
INVESTIGATION OF ANTIMICROBIAL PROPERTIES OF PET-AUNP SCAFFOLDS

6.1 Overview

This study was performed to investigate the potential antimicrobial effects of AuNP conjugated to PET mesh. The risk of infection with hernia mesh materials is of major concern because infection has been shown to cause complications resulting in herniation recurrence and biofilm formation. Even with antibiotic treatment, infection sometimes cannot be eradicated without explanting of the mesh. (Brown and Finch, 2010) The fabrication of hernia meshes has been largely experimented with to minimize the risk for infection during surgical implantation. Positive results have been shown, specifically for PET meshes, due to their macroporous (pores greater than 75 μm) design. However, most PET meshes are multifilament, allowing them to exhibit flexibility and high tensile strength, but also providing small spaces for bacteria to become entrapped and survive unchallenged.

Although research involving nanoparticles as antimicrobial agents is currently a trending topic, bacteria response to AuNP, specifically bare AuNP, has not been extensively researched. In this investigation, PET and PET-AuNP scaffolds were exposed to *Pseudomonas aeruginosa* to evaluate the ability of AuNP to act as an antimicrobial agent when conjugated to PET mesh. *P. aeruginosa* is an opportunistic human pathogen and is commonly encountered in hospital-acquired infections, thus making it a viable choice for this study. (Elswaifi et al., 2009) In past literature,

antimicrobial agents shown to reduce growth of *P. aeruginosa* also showed resistance to other bacteria such as *Staphylococcus aureus* and *Staphylococcus epidermidis.* (Jou et al., 2007)

6.2 Materials and Methods

6.2.1 Materials

- *Pseudomonas aeruginosa* – Ward's Natural Science, Rochester, NY
- Trypto soy broth (TSB) – Alpha Biosciences, Baltimore, MD
- Phosphate buffered saline (PBS) – MP Biomedicals, Solon, OH
- Paraformaldehyde – Electron Microscopy Sciences, Hatfield, PA
- Glutaraldehyde – Electron Microscopy Sciences, Hatfield, PA
- Cacodylate – Electron Microscopy Sciences, Hatfield, PA

6.2.2 Preparation of Pseudomonas aeruginosa for bacteria culture

The *P. aeruginosa* cell line was used to study the bacteria response to PET and PET-AuNP scaffolds. The stock bacteria concentration was established to be roughly 10^8 colony forming units per mL (CFU/mL). A series dilution of the stock bacteria in 1x TSB was performed to yield a concentration of roughly 100 CFU/mL to be used in the bacteria study. All bacteria solution preparation was performed courtesy of Dr. Byung-Doo Lee under the advisement of Dr. Shramik Sengupta.

6.2.3 Investigation of bacteria presence by most probable number method

The initial investigation of the antimicrobial effects of AuNP conjugated to PET mesh was performed with the most probable number (MPN) method. In this experiment, pristine PET was used as the control group and PET-AuNP scaffolds with AuNP concentrations of 0.25x, 0.5x, and 1x were used as the experimental groups. Four repetitions of each scaffold group were used. The PET and PET-AuNP scaffolds were sterilized with a steam autoclave for 35 minutes at 121°C before being placed into individual wells of a 24-well plate. Each scaffold well was then seeded with roughly 100 CFU/mL of *P. aeruginosa* in 0.1x TSB. The scaffolds and bacteria solution were incubated at 37°C and 10% CO_2 for 24 hours. After 24 hours, the solutions from two wells of each scaffold group were removed and transferred to individual micro-centrifuge tubes. The well plate was then placed back in the incubator to allow the remaining scaffolds and solutions to incubate for 48 additional hours. A five step series dilution was performed for each *P. aeruginosa*/TSB solution in 1x TSB. The series diluted solutions were then placed in a shaker incubator (37°C and 100 rpm) for 24 hours before results were observed. The series dilution procedure was repeated for the solutions incubated for 72 hours.

6.2.4 Investigation of bacteria presence by plate counting method

In order to assess the potential antimicrobial effects of the PET-AuNP scaffolds in a more quantitative manner, a bacteria study using the plate counting method was performed. The control and experimental groups remained the same as in the MPN study

and the 24-well plate was prepared with the exact procedure as described in section 6.2.3. After 24 hours of incubation, the solutions from two wells of each of the scaffold groups were removed and diluted. A four step series dilution of the bacteria/TSB solution was performed in 1x PBS. 100 µL of the series diluted solutions were then plated onto individual agar plates and incubated at 37°C and 10% CO_2 for 24 hours. Following the 24 hour incubation, the plates were removed and bacteria colony forming units were manually counted. For the scaffolds incubated for 72 hours, a seven step series dilution was performed on each solution. The fifth, sixth, and seventh dilutions were then plated and incubated for 24 hours before counting.

6.2.5 SEM analysis of PET-AuNP scaffolds with Pseudomonas aeruginosa

Following the 24 and 72 hour exposures of the PET and PET-AuNP scaffolds to *P. aeruginosa*, the scaffolds were removed and rinsed with 1x PBS. The scaffolds were stored in 1x PBS until analysis with SEM was performed. Prior to imaging with the SEM, the scaffolds were exposed to a fixative solution (2% paraformaldehyde and 2% glutaraldehyde in 0.1 M cacodylate buffer) to fixate the bacteria to the surface and then gently rinsed in ultrapure water to remove any salts. Each scaffold was then blotted dry before being placed into the microscope. The Quanta™ 600 SEM in the University of Missouri Electron Microscopy Core was used to image the PET and PET-AuNP scaffolds with attached bacteria. Micrographs were then analyzed to assess the placement of attached bacteria and investigate the effects of AuNP on bacteria attachment to the PET mesh.

6.3 Results and Discussion

6.3.1 Antimicrobial assay with MPN method

The results obtained with the MPN method for assessing the antimicrobial properties of AuNP conjugated to PET mesh did not provide any significant results. The principle of the MPN method is that the presence of bacteria in the solution will produce a cloudy appearance of the solution after incubation. The amount of bacteria present is qualitatively assessed by the degree of cloudiness of the solution. In this investigation, all micro-centrifuge tubes were found to be cloudy and the differences between samples were negligible. These results were consistent for the samples incubated for 24 hours as well as the samples incubated for 72 hours. Due to the principle of this method, as little as one bacterium present in the solution could cause enough proliferation to cloud the solution. It is improbable to expect that AuNP conjugated to PET mesh would have enough long-term antimicrobial properties to eliminate all bacteria present in the culture. Therefore, it was determined that a more precise method was needed to analyze the antimicrobial effects of the PET-AuNP scaffolds.

6.3.2 Antimicrobial assay with plate counting method

Based on the inconclusive results of the MPN bacteria study, the assay was repeated using plate counting to quantify the results. For the scaffolds incubated with bacteria solution for 24 hours, four series dilutions were performed and plated. After a 24 hour incubation of the agar plates, the bacteria had proliferated to the point of being uncountable. Even at the fourth dilution, the plates were nearly confluent with colony

forming units. The plates corresponding to the different scaffold groups were compared against each other and a visual difference was not discernable between the experimental groups.

For the scaffolds incubated for 72 hours, seven series dilutions were performed for each sample solution. Based on the high number of colony forming units observed with the 24 hour samples, only the fifth, sixth, and seventh dilutions were plated for the 72 hour samples. Following the 24 hour incubation, the bacteria colonies were counted and the results are shown in Figures 30 and 31. It can be seen from the graphs that the PET mesh conjugated to AuNP showed less colony forming units than the pristine PET at both the fifth and sixth dilutions. However, a one-way ANOVA determined no significant difference between the means of the scaffold groups at either dilution. No bacteria colonies were found on any of the PET-AuNP scaffold plates at the seventh dilution and only one colony was formed on the PET plates.

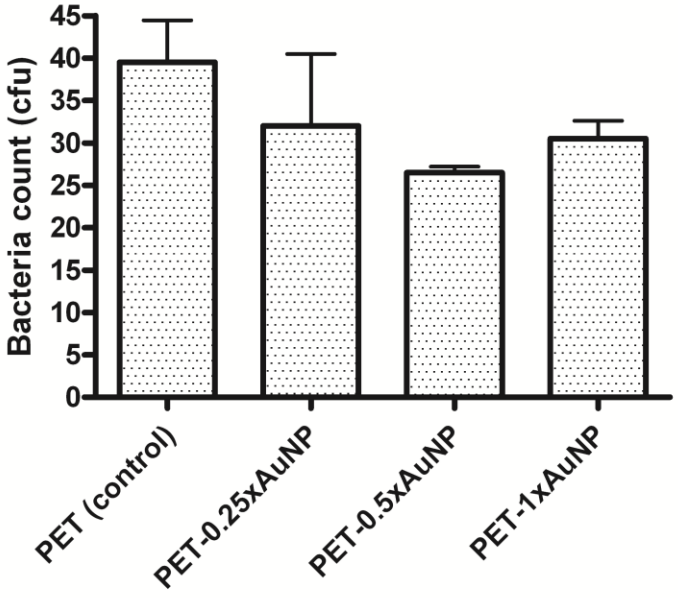

Figure 30. Bacteria count for the fifth dilution of the *P. aeruginosa* solution exposed to scaffolds for 72 hours.

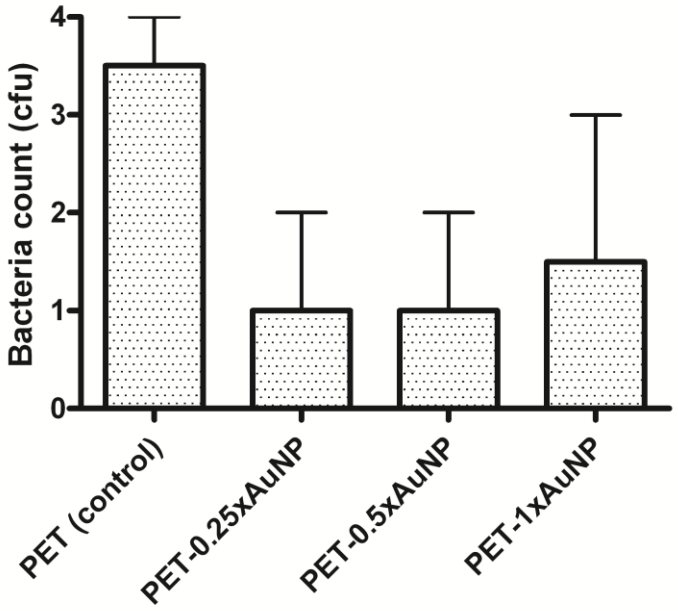

Figure 31. Bacteria count for the sixth dilution of the *P. aeruginosa* solution exposed to scaffolds for 72 hours.

Although statistical analysis did not show significance in the reduction of *P. aeruginosa* by the PET-AuNP scaffolds in comparison to the pristine PET mesh, these initial results show the potential for AuNP to possess antimicrobial properties. Based on the results from the solutions removed after 24 hours, the bacteria count of the solutions incubated for 72 hours was expected to be extremely high. This did not seem to be the case, as the fifth dilutions showed less than 50 colony forming units per plate. To more precisely analyze the long-term antimicrobial effects of the PET-AuNP scaffolds, the 72 hour incubations should be repeated with all dilutions being plated.

6.3.3 SEM analysis of PET-AuNP scaffolds with Pseudomonas aeruginosa

SEM images were obtained for pristine PET and PET-1xAuNP scaffolds exposed to *P. aeruginosa* for 72 hours. Images for each scaffold were taken at several locations and magnifications to ensure a thorough surface analysis of the sample. Results obtained for the control group, pristine PET, are shown in Figures 32 – 34. The pristine PET scaffolds showed several bacteria colonies, adhered to the filament surface as well as embedded between the filaments. These results were expected based on literature showing complications with infection risk in multifilament hernia mesh materials. Additional images of the bacteria exposed PET scaffolds are available in Appendix A.

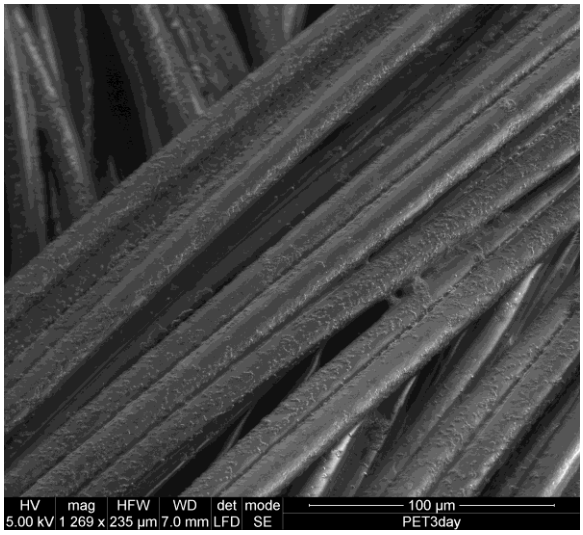

Figure 32. SEM image of pristine PET after 72 hours exposure to *P. aeruginosa*.

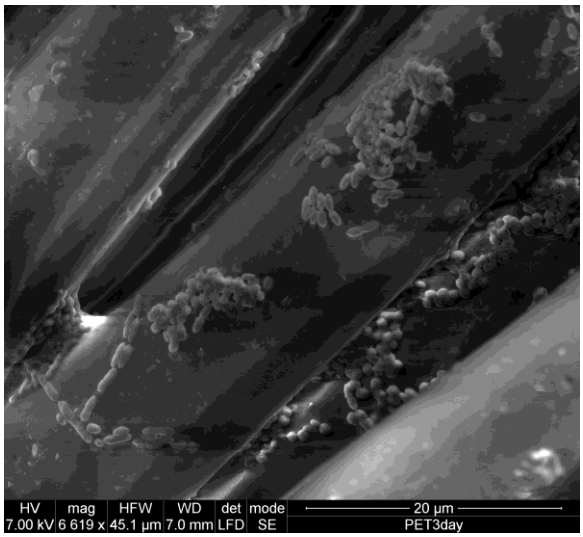

Figure 33. SEM image of pristine PET with bacterial colonies formed on the filament surface.

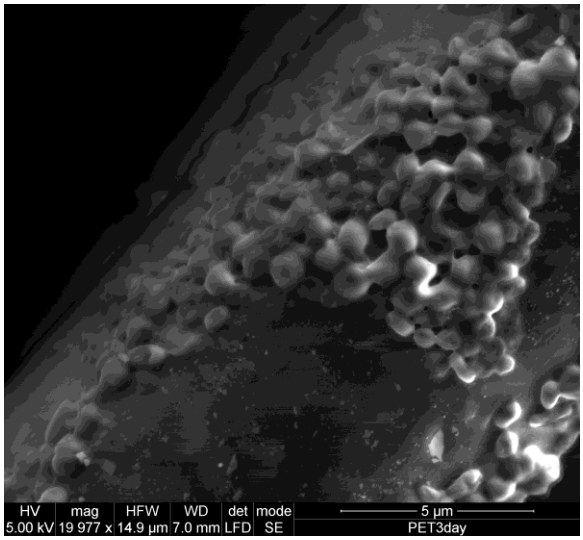

Figure 34. SEM image of *P. aeruginosa* colony formed on pristine PET surface.

Results obtained for the bacteria exposed PET-1xAuNP scaffolds are shown in Figures 35 – 37. It can be seen from the images that significantly less bacteria seem to be present on the AuNP conjugated PET mesh. The majority of the bacteria adhesion observed for the PET-1xAuNP scaffolds appeared to be embedded into the spaces between the polyester filaments; however, on the AuNP covered surface of the filaments, little to no bacteria were observed. These results suggest that conjugation of AuNP to PET could have antimicrobial effects against *P. aeruginosa* colonies and therefore be used to potentially reduce infection risk in PET hernia meshes. EDS analysis was also performed on the bacteria exposed PET-1xAuNP scaffolds to ensure the presence of gold on the surface (Figure 38). It is also important to note that salts were not identified by EDS to be present on the PET surface, indicating that all the charged particles observed on the SEM micrograph were gold.

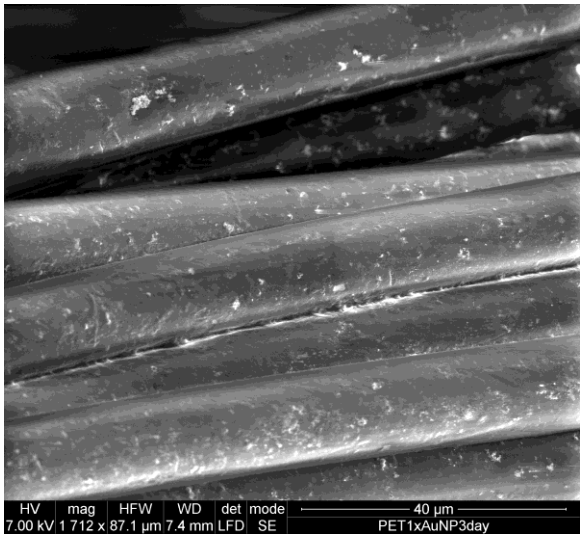

Figure 35. SEM image of PET-1xAuNP scaffold after 72 hours exposure to *P. aeruginosa.*

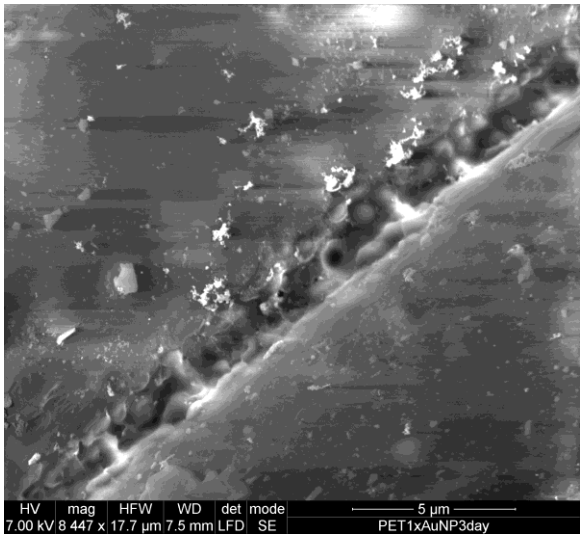

Figure 36. SEM image of bacteria colonies in between filaments on a PET-1xAuNP scaffold.

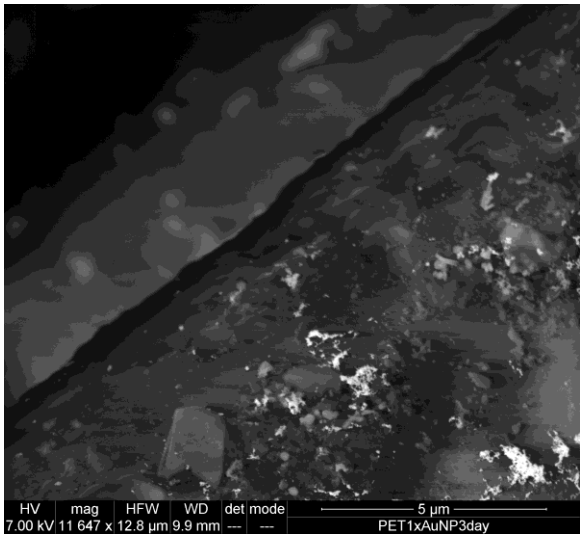

Figure 37. SEM image of PET-1xAuNP surface after 72 hours exposure to *P. aeruginosa.*

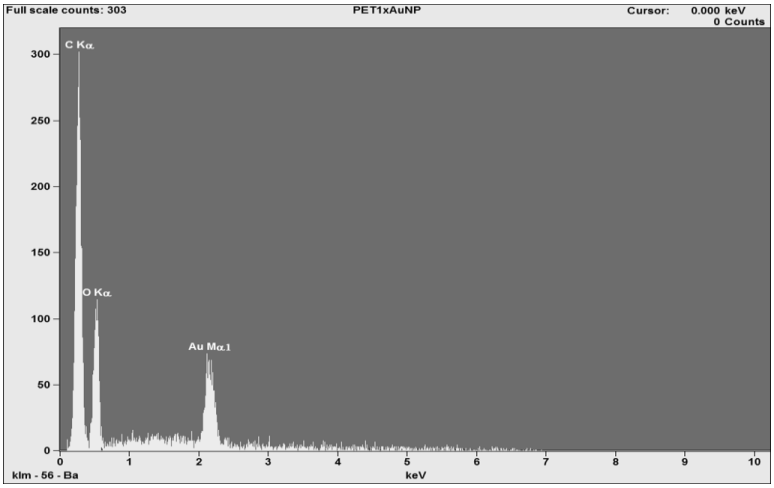

Figure 38. EDS spectrum of full surface scan of PET-1xAuNP after bacteria exposure.

6.4 Conclusion

This study showed that AuNP conjugated to PET mesh has potential to exhibit antimicrobial effects but needs to be further investigated. The MPN and bacteria

counting experiments were limited in the fact that the antimicrobial analysis was being performed on the bulk solution surrounding the scaffolds. More specifically, the AuNP could have significant antimicrobial properties against bacteria in contact with the mesh but not be able to significantly reduce long-term bacteria. As the risk for infection with multifilament hernia meshes concentrates on bacteria entrapped within the filaments of the mesh, being able to reduce the growth of bacteria on the surface would be a more relevant property.

Results obtained from the investigation of adhered bacteria to the PET surface through SEM analysis showed further support for the suggestion of AuNP possessing antimicrobial properties. SEM images of the pristine PET samples showed much higher amounts of bacteria in comparison to the PET-1xAuNP scaffolds. More specifically, the outer surface of an individual filament of pristine PET was shown to be covered with bacterial colonies, whereas the surface of a AuNP covered filament was shown to be nearly void of bacteria. This observation strongly supports the hypothesis that AuNP possess antimicrobial effects, as the outer filament surface is likely to be more covered with nanoparticles than the space in between the filaments. Additionally, while there were bacteria present in between the filaments for both scaffold groups, a lesser amount was observed for the PET-1xAuNP scaffold. This surface analysis data, along with preliminary results from the bacteria counting study, suggest that an AuNP conjugated scaffold could reduce the infection risk of PET hernia meshes.

APPENDIX A
ADDITIONAL FIGURES

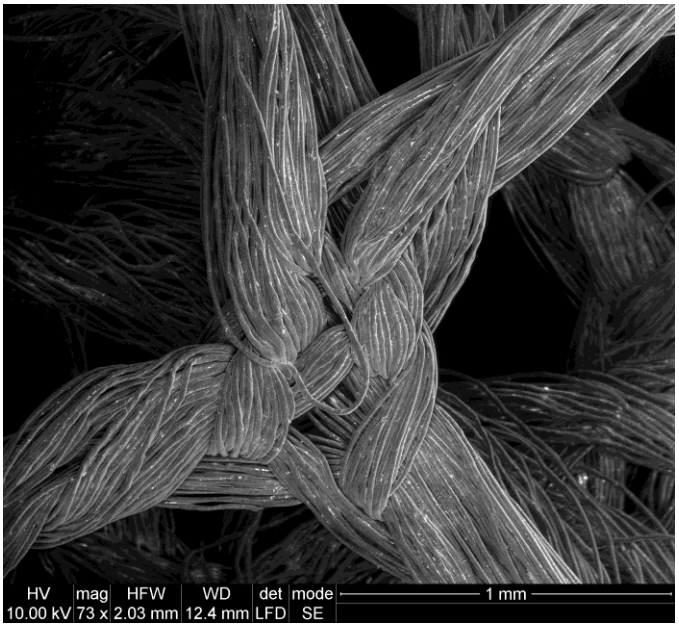

Figure 1. SEM image of Parietex™ 3D PET-0.1xAuNP scaffold.

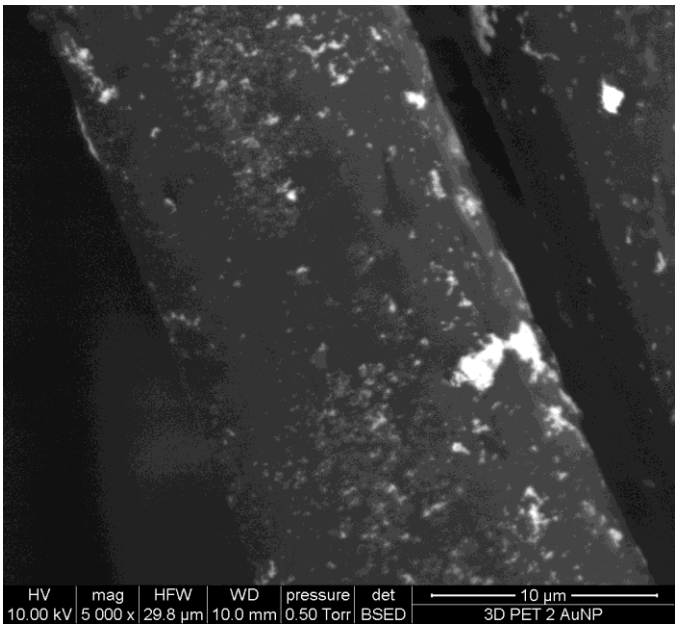

Figure 2. SEM image of Parietex™ 3D PET-1xAuNP scaffold.

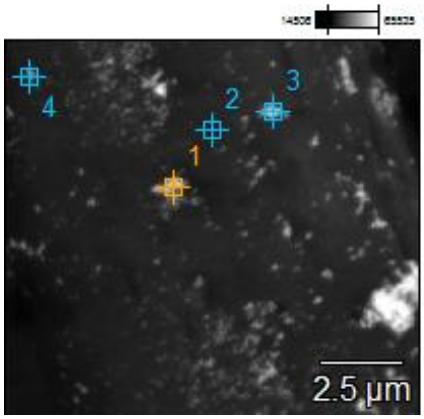

Figure 3. SEM image of Parietex™ 3D PET-1xAuNP scaffold with selected points for EDS analysis.

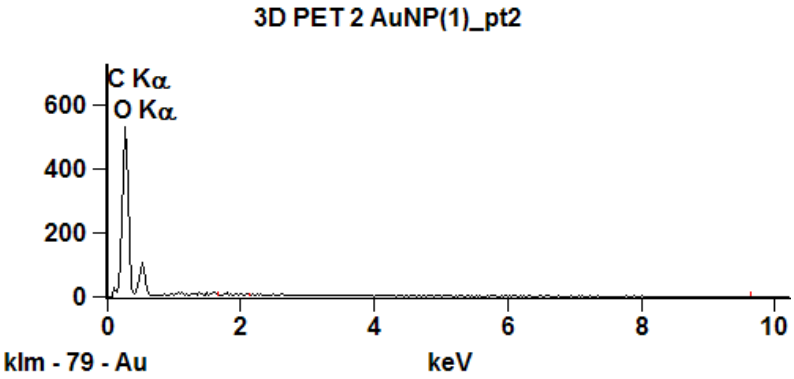

Figure 4. EDS analysis for point 2 on the SEM image.

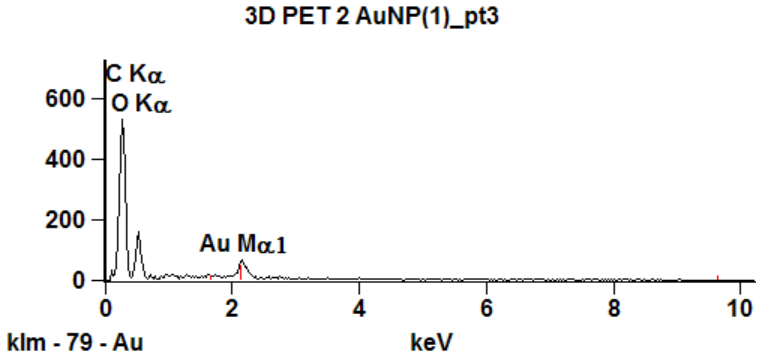

Figure 5. EDS analysis for point 3 on the SEM image. Au identified by the peak at around 2.14 keV.

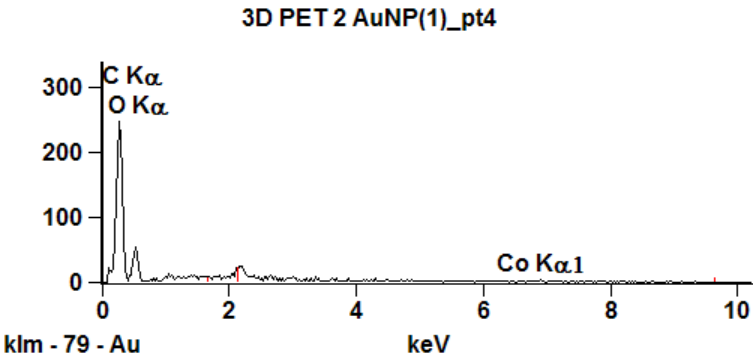

Figure 6. EDS analysis for point 4 on SEM image.

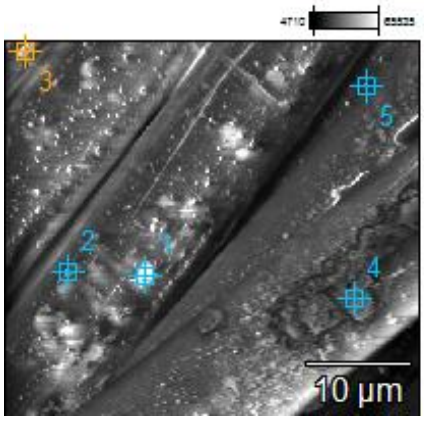

Figure 7. SEM image of Parietex™ 3D PET-0.5xAuNP scaffold with points selected for EDS analysis.

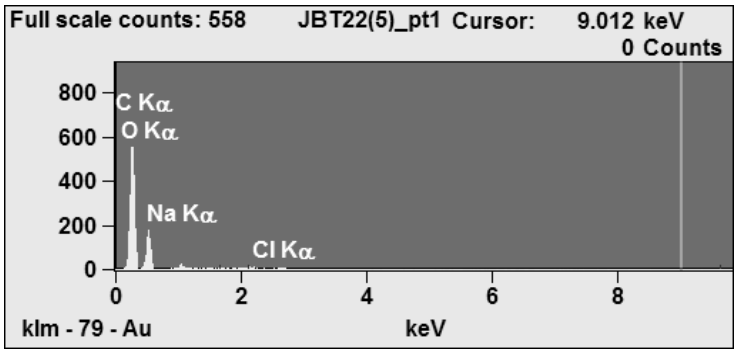

Figure 8. EDS analysis for point 1 on SEM image.

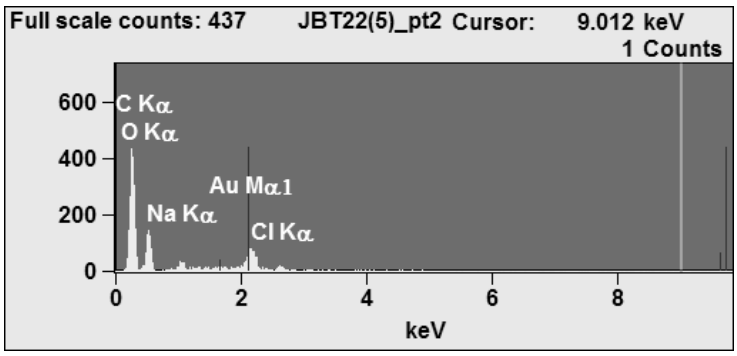

Figure 9. EDS analysis for point 2 on SEM image. Au identified by the peak at 2.14 keV.

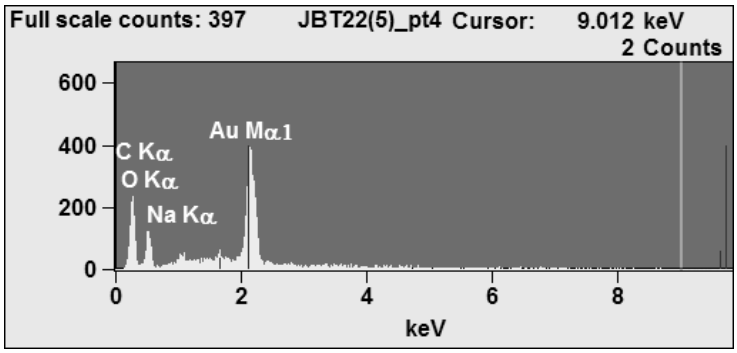

Figure 10. EDS analysis for point 4 on SEM image. Prominent peak at 2.14 keV suggests agglomeration of AuNP.

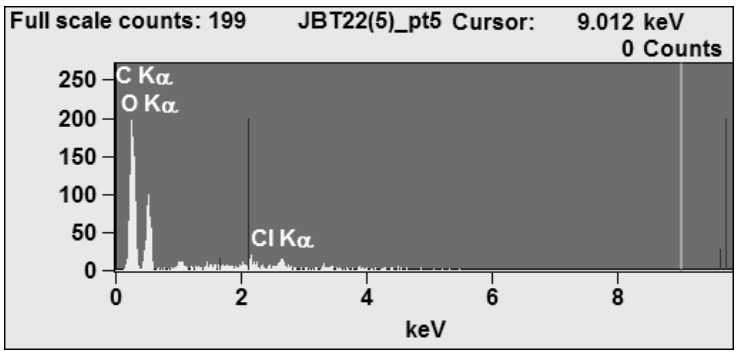

Figure 11. EDS analysis for point 5 on SEM image.

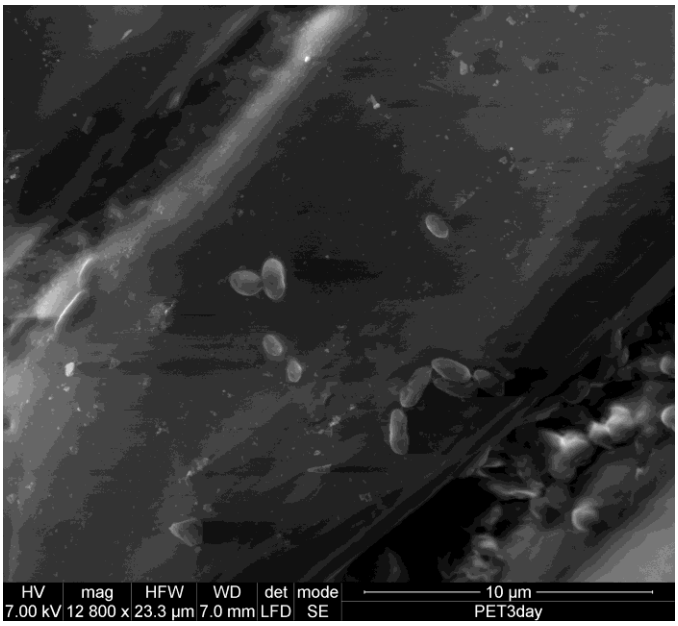

Figure 12. SEM image of pristine PET exposed to *P. aeruginosa* for 72 hours.

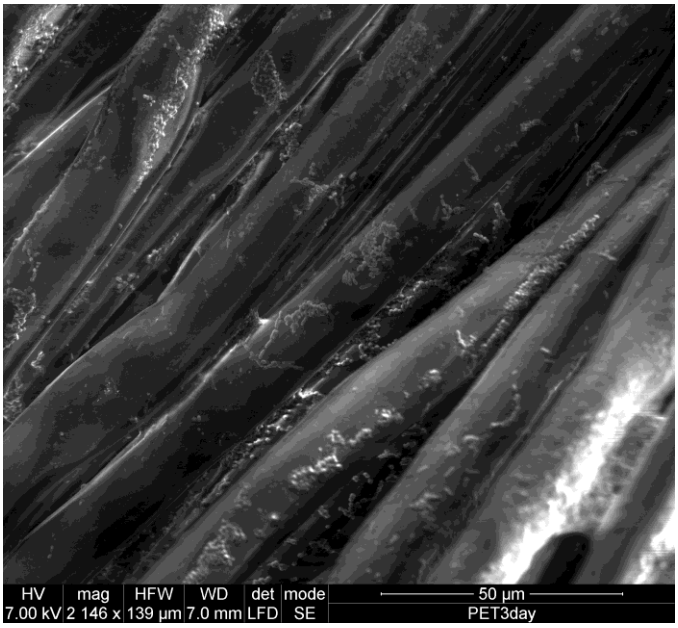

Figure 13. SEM image of pristine PET exposed to *P. aeruginosa* for 72 hours.

APPENDIX B
THERMAL ANALYSIS OF PET-AUNP SCAFFOLDS USING DIFFERENTIAL SCANNING CALORIMETRY

1. Overview

This purpose of this study was to analyze the thermal properties of PET mesh conjugated to AuNP and compare the results with those obtained for pristine PET. Thermal analysis was performed using modulated differential scanning calorimetry (DSC) and used to assess the effects of chemical carboxylation and AuNP conjugation on the thermal stability of PET. The onset temperature, denaturation temperature, and thermal heat of fusion were determined for AuNP conjugated PET and compared to respective values for pristine PET.

2. Materials and Methods

2.1 Preparation of samples for DSC testing

PET, PET-0.5xAuNP, and PET-1xAuNP scaffolds were used in the DSC analysis. Samples from each group were cut into approximately 4 mm x 4 mm squares and weighed before being hermetically sealed in Tzero aluminum pans. Each empty pan and lid were initially weighed, loaded with a mesh sample, sealed, and then weighed again to verify the weight of the test sample. A minimum of four samples for each experimental group were prepared for DSC testing.

2.2 Thermal analysis of samples using DSC

Thermal analysis was performed by a differential scanning calorimeter (Q2000, TA Instruments, New Castle, DE) using modulated DSC heat only with a modulation period of 80 seconds and a ramp rate of 5°C per minute. A start temperature of -90°C and final temperature of 300°C were used for the PET samples.

2.3 Quantification and calculation of thermal properties

DSC curves were analyzed using TA Universal Analysis software. The onset temperature and denaturation temperature of each sample were determined by the limits of the melting peak on the DSC curve. The area of the melting peak was then integrated to calculate the thermal heat of fusion. Values for each sample's thermal properties were analyzed with GraphPad Prism® software to determine statistical relevance between the experimental groups.

3. Results and Discussion

3.1 Thermal analysis of PET-AuNP scaffolds

The thermal stability of the PET mesh can be visualized by a plot of the DSC analysis, as shown in Figure 1. The onset temperature and heat of fusion are shown to the left of each sample's melting peak and then denaturation temperature is shown to the right of the peak.

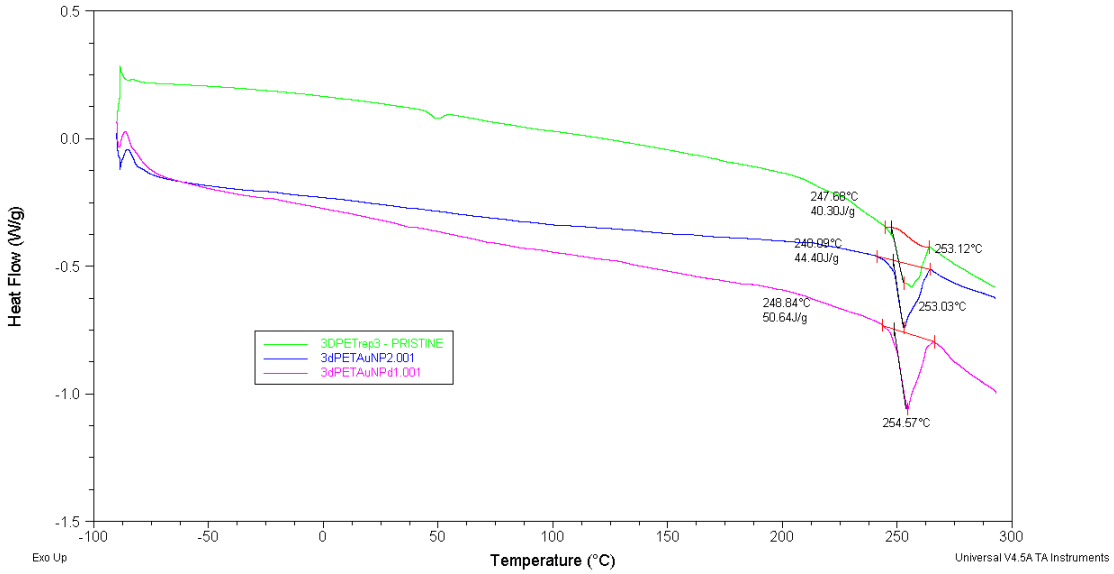

Figure 1. DSC curves for pristine PET (green), PET-1xAuNP (blue), and PET-0.5xAuNP (pink).

3.2 Statistical analysis of thermal properties

Statistical analysis was performed for each of the thermal properties to determine if there were any significant differences between the three PET groups. One-way ANOVA tests did not show statistical significant differences for any of the thermal properties analyzed. These results indicated that the thermal stability of the PET-AuNP scaffolds was comparable to that of the pristine PET mesh, suggesting that the modification procedures did not significantly affect the PET's resistance to thermal degradation.

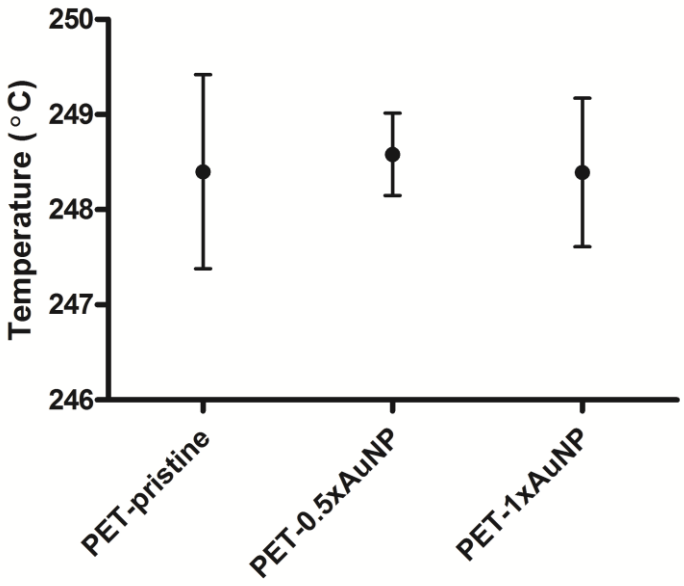

Figure 2. Comparison of onset temperatures for PET mesh.

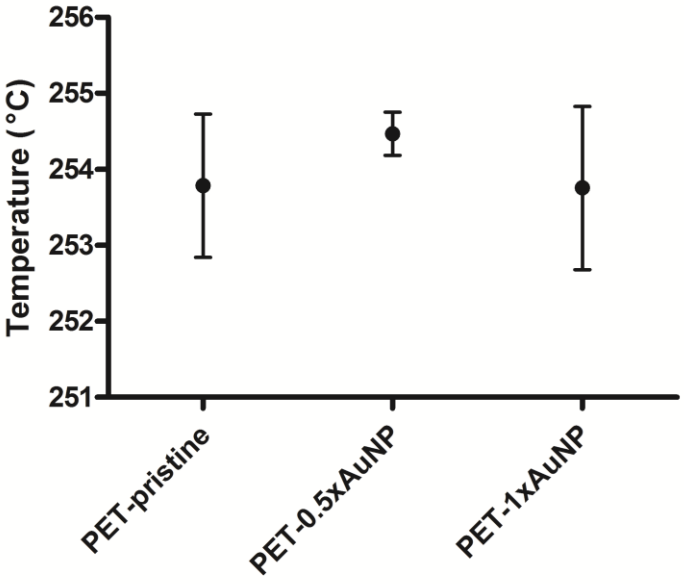

Figure 3. Comparison of denaturation temperatures for PET mesh.

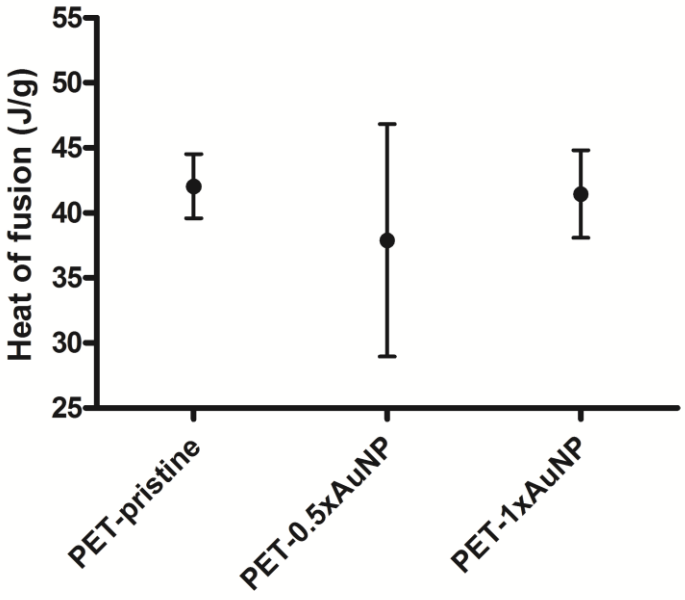

Figure 4. Heat of fusion values for PET mesh.

4. Conclusion

Analysis of the thermal transitions of PET and PET-AuNP scaffolds showed values approximately similar for each experimental group. These results indicated that neither the chemical carboxylation nor the AuNP cross-linking procedures used to modify the PET surface had a significant effect on the bulk thermal properties of the pristine PET.

APPENDIX C
ANALYSIS OF CELL ATTACHMENT TO PET-AUNP SCAFFOLDS

1. Overview

The objective of this investigation was to analyze the cellular attachment of L929 cells to the PET and PET-AuNP scaffolds. This study was based on the principle used in the WST-1 assays in Chapter 4, but focused on quantifying only the amount of cells adherent to the scaffolds after the seven day cell culture.

2. Materials and Methods

The materials and preparation procedures used were the same as was described in Chapter 4 for the seven day cell culture assay. Pristine PET mesh (Parietex™ Flat Sheet Mesh, 3D weave) was used in the control group and PET-AuNP scaffolds in varying concentrations (0.3x, 0.5x, 1x) were used as the experimental test groups. The protocol for analyzing the cell attachment to the scaffolds was adapted from a study performed by Zhang et al. (2008). Following the seven day exposure of L929 cells to the PET and PET-AuNP scaffolds, the scaffolds were removed from the 24-well plate and transferred to a clean well plate. Each scaffold was then washed three times with DPBS to remove all unattached cells from the mesh. 0.5 mL of sterile culture medium and 50 µL of WST-1 reagent were added to each scaffold well and incubated for one, two, and three hour time periods. The quantification of the WST-1 cell attachment assay was performed

exactly the same as in section 4.2.4 by measuring the absorbance of the culture medium/WST-1 reagent.

3. Results and Discussion

Absorbance values obtained from the microplate reader showed results largely different from those found in the original WST-1 assays. After one hour of incubation of the scaffolds with WST-1 reagent, the pristine PET exhibited the highest absorbance, suggesting the greatest amount of cell attachment. Both the PET-0.5xAuNP and PET-1xAuNP scaffold groups showed values significantly lower (P value < 0.01) than those of the control PET group. The statistical differences were determined by a one-way ANOVA and Tukey's multiple comparison test. However, after the two and three hour incubations, the trend seemed to shift and the absorbance values of the PET-1xAuNP started to level out with the pristine PET.

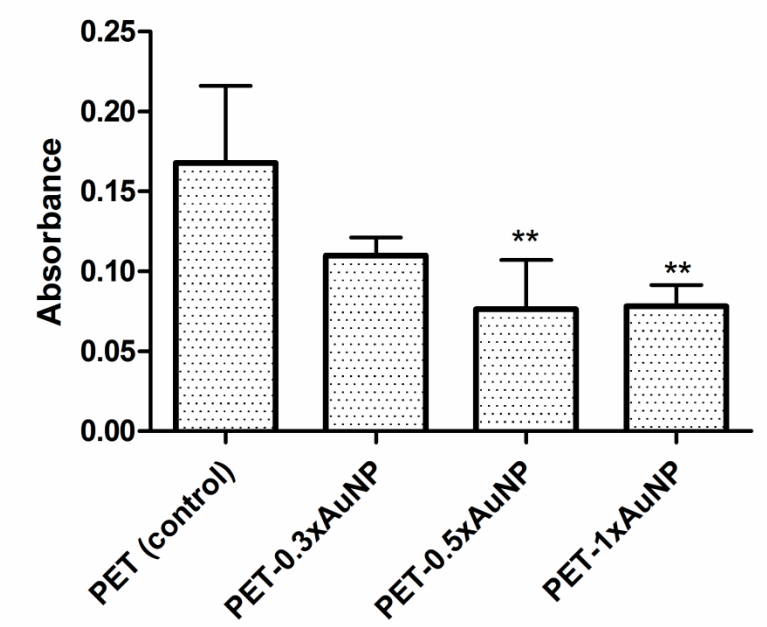

Figure 1. Absorbance values after 1 hour incubation.
**** Significantly different from PET (control), P<0.01**

Table 1. P values for ANOVA of 1 hour WST-1 assay

PET (control) vs. PET-0.3xAuNP	P > 0.05
PET (control) vs. PET-0.5xAuNP	P < 0.01
PET (control) vs. PET-1xAuNP	P < 0.01
PET-0.3xAuNP vs. PET-0.5xAuNP	P > 0.05
PET-0.3xAuNP vs. PET-1xAuNP	P > 0.05
PET-0.5xAuNP vs. PET-1xAuNP	P > 0.05

Samples observed after two hours of incubation with the WST-1 reagent followed the same general trend of the absorbance values from the one hour WST-1 incubation. It should be noted, however, that after the two hour incubation, cell attachment on the PET-0.5xAuNP scaffolds was found to be significantly lower than the pristine PET with a

99% confidence interval, whereas cell attachment on the PET-1xAuNP scaffolds was shown to be significantly lower only with a confidence interval of 95%.

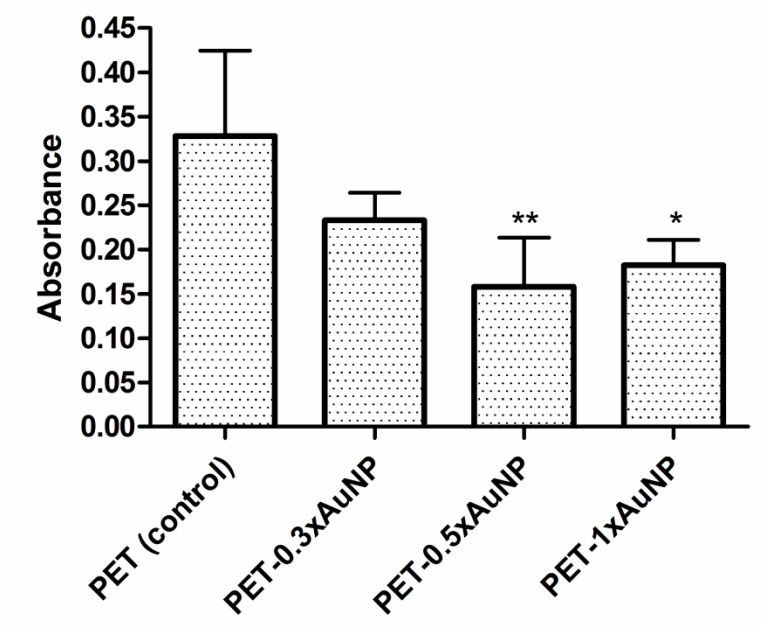

Figure 2. Absorbance values after 2 hour incubation.
***Significant decrease from PET (control), P<0.05**
****Significant decrease from PET (control), P<0.01**

Table 2. P values for ANOVA of 2 hour WST-1 assay

PET (control) vs. PET-0.3xAuNP	P > 0.05
PET (control) vs. PET-0.5xAuNP	P < 0.01
PET (control) vs. PET-1xAuNP	P < 0.05
PET-0.3xAuNP vs. PET-0.5xAuNP	P > 0.05
PET-0.3xAuNP vs. PET-1xAuNP	P > 0.05
PET-0.5xAuNP vs. PET-1xAuNP	P > 0.05

Measurements taken after three hours of incubation of the scaffolds with the WST-1 reagent showed additional changes in the absorbance values for the PET-

0.5xAuNP and PET-1xAuNP scaffolds. A one-way ANOVA and Tukey's multiple comparison test determined only the PET-0.5xAuNP scaffold group to have significantly less absorbance than the control PET group. The PET-1xAuNP group was found to have a P value greater than 0.05, which suggested it was no longer significantly lower than the control PET.

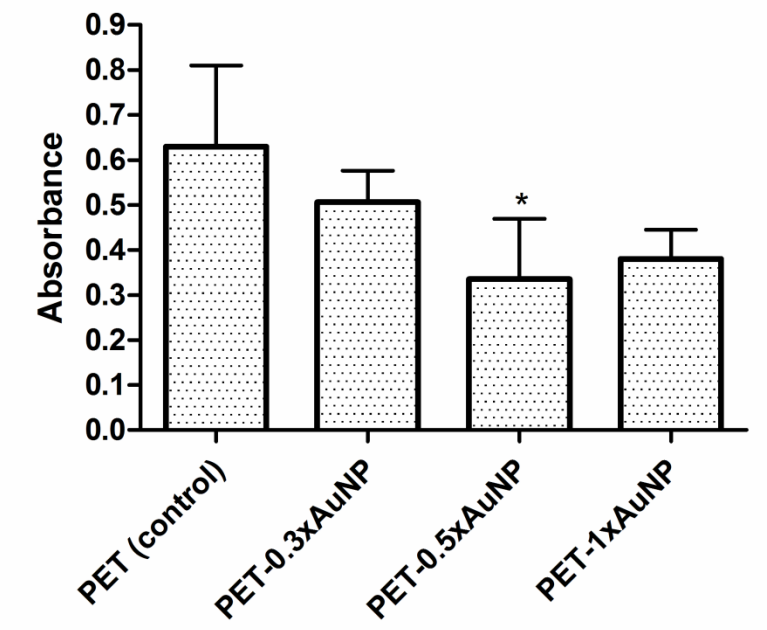

Figure 3. Absorbance values after 3 hour incubation. *Significant decrease from PET (control), P<0.05

Table 3. P values for ANOVA of 3 hour WST-1 assay.

PET (control) vs. PET-0.3xAuNP	P > 0.05
PET (control) vs. PET-0.5xAuNP	P < 0.05
PET (control) vs. PET-1xAuNP	P > 0.05
PET-0.3xAuNP vs. PET-0.5xAuNP	P > 0.05
PET-0.3xAuNP vs. PET-1xAuNP	P > 0.05
PET-0.5xAuNP vs. PET-1xAuNP	P > 0.05

4. Conclusion

At the start of this investigation of cell attachment to the PET and PET-AuNP scaffolds, it was expected that a trend similar to that seen in the traditional WST-1 assay would be observed. Instead, the results showed all PET-AuNP scaffolds to have less absorbance than pristine PET, correlating to a lower amount of viable cells. Since this protocol consisted of washing the scaffolds to allow for quantification of attached cells only, these results suggested that AuNP may have deterred cells from attaching to the PET mesh surface.

Initial data from this cell attachment assay showed results inconsistent with the previous analysis of cell viability of the PET-AuNP scaffolds, which showed the highest absorbance values for cells exposed to the PET-1xAuNP scaffolds. However, the consistent change in results throughout the three incubation times indicate that the WST-1 reagent may still have been reducing and therefore was not a valid indicator of the total number of attached cells. The absorbance values obtained for attached cells only were much lower than absorbance measurements correlating to cell growth in the original culture well with the scaffolds. This cell attachment study should be repeated using a higher concentration of cells to initially seed the assay, as well as three to four hour incubations of the scaffolds with the WST-1 reagent.

REFERENCES

Bringman, S., Conze, J., Cuccurullo, D., Deprest, J., Junge, K., Klosterhalfen, B., Parra-Davila, E., Ramshaw, B., & Schumpelick, V. (2010). Hernia repair: the search for ideal meshes. [10.1007/s10029-009-0587-x]. *Hernia, 14*(1), 81-87.

Brown, C. N., & Finch, J. G. (2010). Which mesh for hernia repair? *Annals of the Royal College of Surgeons of England, 92*(4), 272-278.

Castaneda, L., Valle, J., Yang, N., Pluskat, S., & Slowinska, K. (2008). Collagen Cross-Linking with Au Nanoparticles. [doi: 10.1021/bm800793z]. *Biomacromolecules, 9*(12), 3383-3388.

Christenson, E. M., Anderson, J. M., & Hiltner, A. (2004). Oxidative mechanisms of poly(carbonate urethane) and poly(ether urethane) biodegradation: In vivo and in vitro correlations. *Journal of Biomedical Materials Research Part A, 70A*(2), 245-255.

Clark, D. T., & Wilson, R. (1983). Selective Surface Modification of Polymers by means of Hydrogen and Oxygen Plasmas. *Polymer Chemistry, 21*(3), 837-853.

Connor, E., Mwamuka, J., Gole, A., Murphy, C., & Wyatt, M. (2005). Gold Nanoparticles Are Taken Up by Human Cells but Do Not Cause Acute Cytotoxicity. *Small, 1*(3), 325-327.

Costello, C. R., Bachman, S. L., Ramshaw, B. J., & Grant, S. A. (2007a). Materials characterization of explanted polypropylene hernia meshes. *Journal of Biomedical Materials Research Part B: Applied Biomaterials, 83B*(1), 44-49.

Costello, C. R., Bachman, S. L., Grant, S. A., Cleveland, D. S., Loy, T. S., & Ramshaw, B. J. (2007b). Characterization of Heavyweight and Lightweight Polypropylene Prosthetic Mesh Explants From a Single Patient. *Surgical Innovation, 14*(3), 168-176.

Elswaifi, S. F., Palmieri, J. R., Hockey, K. S., & Rzigalinski, B. A. (2009). Antioxidant Nanoparticles for Control of Infectious Disease. [Article]. *Infectious Disorders - Drug Targets, 9*(4), 445-452.

Eriksen, J., Gögenur, I., & Rosenberg, J. (2007). Choice of mesh for laparoscopic ventral hernia repair. *Hernia, 11*(6), 481-492.

Grant, S. A., & Ramshaw, B. J. (2010). Book chapter to be published, obtained through private communication with S. A. Grant.

Gu, Y.-J., Cheng, J., Lin, C.-C., Lam, Y. W., Cheng, S. H., & Wong, W.-T. (2009). Nuclear penetration of surface functionalized gold nanoparticles. [doi: DOI: 10.1016/j.taap.2009.03.009]. *Toxicology and Applied Pharmacology, 237*(2), 196-204.

Hsu, S.-H., Tang, C.-M., & Tseng, H.-J. (2007). Gold Nanoparticles Induce Surface Morphological Transformation in Polyurethane and Affect the Cellular Response. [doi: 10.1021/bm700471k]. *Biomacromolecules, 9*(1), 241-248.

Irena, G., Jolanta, B., & Karolina, Z. (2009). Chemical modification of poly(ethylene terephthalate) and immobilization of the selected enzymes on the modified film. [doi: DOI: 10.1016/j.apsusc.2009.05.126]. *Applied Surface Science, 255*(19), 8293-8298.

Jingrun, R., Jin, W., Hong, S., & Nan, H. (2008). Surface modification of polyethylene terephthalate with albumin and gelatin for improvement of anticoagulation and endothelialization. [doi: DOI: 10.1016/j.apsusc.2008.06.181]. *Applied Surface Science, 255*(2), 263-266.

Joseph, R., Shelma, R., Rajeev, A., & Muraleedharan, C. (2009). Characterization of surface modified polyester fabric. [10.1007/s10856-008-3502-6]. *Journal of Materials Science: Materials in Medicine, 20*(0), 153-159.

Jou, C. H., Lin, S. M., Yun, L., Hwang, M. C., Yu, D. G., Chou, W. L., Lee, J. S., & Yang, M. C. (2007). Biofunctional properties of polyester fibers grafted with chitosan and collagen. *Polymers for Advanced Technologies, 18*(3), 235-239.

Jung, K. H., Huh, M. W., Meng, W., Yuan, J., Hyun, S. H., Bae, J. S., Hudson, S. M., & Kang, I. K. (2007). Preparation and antibacterial activity of PET/chitosan nanofibrous mats using an electrospinning technique. *Journal of Applied Polymer Science, 105*(5), 2816-2823.

Klinge, U., Klosterhalfen, B., Müller, M., & Schumpelick, V. (1999). Foreign Body Reaction to Meshes Used for the Repair of Abdominal Wall Hernias. [Article]. *European Journal of Surgery, 165*(7), 665-673.

Li, J. X., Wang, J., Shen, L. R., Xu, Z. J., Li, P., Wan, G. J., & Huang, N. (2007). The influence of polyethylene terephthalate surfaces modified by silver ion implantation on bacterial adhesion behavior. [doi: DOI: 10.1016/j.surfcoat.2006.02.069]. *Surface and Coatings Technology, 201*(19-20), 8155-8159.

Liu, Y., Chen, J.-R., Yang, Y., & Wu, F. (2008). Improved blood compatibility of poly(ethylene terephthalate) films modified with L-arginine. [doi:10.1163/156856208783719545]. *Journal of Biomaterials Science, Polymer Edition, 19*, 497-507.

Liu, Y., He, T., & Gao, C. (2005). Surface modification of poly(ethylene terephthalate) via hydrolysis and layer-by-layer assembly of chitosan and chondroitin sulfate to construct cytocompatible layer for human endothelial cells. [doi: DOI: 10.1016/j.colsurfb.2005.09.005]. *Colloids and Surfaces B: Biointerfaces, 46*(2), 117-126.

Liu, Y., Yang, Y., & Wu, F. (2010). Effects of l-arginine immobilization on the anticoagulant activity and hemolytic property of polyethylene terephthalate films. [doi: DOI: 10.1016/j.apsusc.2010.01.060]. *Applied Surface Science, 256*(12), 3977-3981.

Muthuvijayan, V., Gu, J., & Lewis, R. S. (2009). Analysis of functionalized polyethylene terephthalate with immobilized NTPDase and cysteine. [doi: DOI: 10.1016/j.actbio.2009.05.020]. *Acta Biomaterialia, 5*(9), 3382-3393.

Pernodet, N., Fang, X., Sun, Y., Bakhtina, A., Ramakrishnan, A., Sokolov, J., Ulman, A., & Rafailovich, M. (2006). Adverse Effects of Citrate/Gold Nanoparticles on Human Dermal Fibroblasts. *Small, 2*(6), 766-773.

Qu, Y., & Lü, X. (2009). Aqueous Synthesis of Gold Nanoparticles and their Cytotoxicity in Human Dermal Fibroblasts – Fetal. [doi: 10.1088/1748-6041/4/2/025007]. *Biomedical Materials, 4*(2), 1-5.

Rai, A., Prabhune, A., & Perry, C. C. (2010). Antibiotic mediated synthesis of gold nanoparticles with potent antimicrobial activity and their application in antimicrobial coatings. *Journal of Materials Chemistry, 20*(32), 6789-6798.

Sandberg, T., Karlsson Ott, M., Carlsson, J., Feiler, A., & Caldwell, K. D. (2009). Potential use of mucins as biomaterial coatings. II. Mucin coatings affect the conformation and neutrophil-activating properties of adsorbed host proteins—Toward a mucosal mimic. *Journal of Biomedical Materials Research Part A, 91A*(3), 773-785.

Takke, V., Behary, N., Perwuelz, A., & Campagne, C. (2009). Studies on the atmospheric air–plasma treatment of PET (polyethylene terephtalate) woven fabrics: Effect of process parameters and of aging. *Journal of Applied Polymer Science, 114*(1), 348-357.

Thonemann, B., Schmalz, G., Hiller, K. A., & Schweikl, H. (2002). Responses of L929 mouse fibroblasts, primary and immortalized bovine dental papilla-derived cell lines to dental resin components. [doi: DOI: 10.1016/S0109-5641(01)00056-2]. *Dental Materials, 18*(4), 318-323.

Voskerician, G., Jin, J., White, M., Williams, C., & Rosen, M. (2010). Effect of biomaterial design criteria on the performance of surgical meshes for abdominal hernia repair: a pre-clinical evaluation in a chronic rat model. *Journal of Materials Science: Materials in Medicine, 21*(6), 1989-1995.

Yang, L., Chen, J., Guo, Y., & Zhang, Z. (2009). Surface modification of a biomedical polyethylene terephthalate (PET) by air plasma. [doi: DOI: 10.1016/j.apsusc.2008.11.048]. *Applied Surface Science, 255*(8), 4446-4451.

Yang, Z., Belu, A. M., Liebmann-Vinson, A., Sugg, H., & Chilkoti, A. (2000). Molecular Imaging of a Micropatterned Biological Ligand on an Activated Polymer Surface. [doi: 10.1021/la0000623]. *Langmuir, 16*(19), 7482-7492.

Zhang, W., Yi, X., Sun, X., & Zhang, Y. (2008). Surface modification of non-woven poly (ethylene terephthalate) fibrous scaffold for improving cell attachment in animal cell culture. *Journal of Chemical Technology & Biotechnology, 83*(6), 904-911.

Zhu, A. P., Zhao, F., & Fang, N. (2008). Regulation of vascular smooth muscle cells on poly(ethylene terephthalate) film by O-carboxymethylchitosan surface immobilization. *Journal of Biomedical Materials Research Part A, 86A*(2), 467-476.

Zieren, J., Neuss, H., Paul, M., & Müller, J. (2004). Introduction of polyethylene terephthalate mesh (KoSa hochfest®) for abdominal hernia repair: An animal experimental study. [Article]. *Bio-Medical Materials & Engineering, 14*(2), 127-132.